

# **Journal of Electrical Engineering and Modern Technology**

**Volume No. 12**

**Issue No. 1**

**January - April 2024**



**ENRICHED PUBLICATIONS PVT. LTD**

**S-9, IInd FLOOR, MLU POCKET,  
MANISH ABHINAV PLAZA-II, ABOVE FEDERAL BANK,  
PLOT NO-5, SECTOR-5, DWARKA, NEW DELHI, INDIA-110075,  
PHONE: - + (91)-(11)-47026006**

# **Journal of Electrical Engineering and Modern Technology**

## **Aims and Scope**

Journal of Electrical engineering and Modern Technology, publishes original research papers in the fields of Electrical and Electronic Engineering and in related disciplines. Areas included (but not limited to) are electronics and communications engineering, electric energy, automation, control and instrumentation, computer and information technology, and the electrical engineering aspects of building services and aerospace engineering. Journal publishes research articles and reviews within the whole field of electrical and electronic engineering, new teaching methods, curriculum design, assessment, validation and the impact of new technologies and it will continue to provide information on the latest trends and developments in this ever-expanding subject.

# **Journal of Electrical Engineering and Modern Technology**

**Managing Editor  
Mr. Amit Prasad**

**Editorial Board Member**

**S. Gajendran**  
Associate Professor/Production  
Engineering  
MIT, Anna University, Chennai,  
India  
[gajendrasm@gmail.com](mailto:gajendrasm@gmail.com)

# Journal of Electrical Engineering and Modern Technology

(Volume No. 12, Issue No. 1, January - April 2024)

## Contents

Sr. No	Article/ Autors	Pg No
01	Thermodynamic Investigation Of A Biomass Felled Gasification For Combined Production Of Power And Refrigeration <i>- Mohd Parvez , Tasmeeem A Khan</i>	01-14
02	Refrigeration using Green Secondary Refrigerant (Ice Slurries) - Some Studies on Ice Slurries and Scraped Surface Ice Slurry Generator <i>-Dr. Rajinder Singh</i>	15-23
03	Comparison of Fourth Generation Refrigerants HFO 1234 yf and 1234ze by Second Law Efficiency and Exergy Destruction Analysis for Automobile Sector <i>- Salma Khatoon</i>	24-34
04	Choice Of Static Var Compensator (SVC), Modeling And Determination Of Its Power Factor Correction (PFC) Capability In A.C. Transmission Line <i>- Ibekwe B.E., Chiwetalu U. J., Eje, B.E</i>	35-40
05	Self Heating Effects In Soi Technology <i>- Prem Prakash Satpathy, Dr. Vijay Nath, Abhinandan Jain</i>	41-47

---

---

# Thermodynamic Investigation Of A Biomass Felled Gasification For Combined Production Of Power And Refrigeration

**Mohd Parvez<sup>\*1</sup>, Tasmeeem A Khan<sup>2</sup>**

<sup>\*1</sup>Department of Mechanical Engineering, Al-Falah University, Faridabad (Haryana) India

<sup>2</sup>Department of Mechanical Engineering, JMI New Delhi

Email: mparvezalig@rediffmail.com

## **ABSTRACT**

This paper presents the findings of a thermodynamic investigation into the operation of a biomass fuelled gasification cogeneration cycle for the simultaneous production of refrigeration. A thermodynamic analysis through energy and exergy is employed to investigate the effect of gas turbine inlet temperature and steam turbine inlet pressure on performance of the topping integrated gasification combined cycle with ejector at the exit of steam turbine and bottoming ORC with an ejector. It was found that both the efficiencies increases with the employment of ejectors are 8.5% and 5.5% as compared to combined power cycle. Therefore, introducing double ejectors into the integrated gasification combined cycle showed a significant improvement in its thermodynamic performance which gives a new way to the researchers.

*Keywords—biomass, gasification, ejector refrigeration, energy, exergy*

## **1.0 INTRODUCTION**

Energy policy is promoting many researches both for the enhancement of utilization of renewable energy and low enthalpy fuels for power generation and for finding the most effective ways of using them. Biomass is usually considered as a renewable energy source with low or zero life-cycle CO<sub>2</sub> emissions, since the carbon produced in the combustion can be balanced by the formation of new. Therefore, in the future world energy scenario, biomass is expected to play a fundamental role for both greenhouse gas mitigation and traditional fossil-fuels replacement. According to the international energy agency, biomass currently contributes as 14% of the world energy supplies including waste. Biomass can be converted into electric power through several methods. The most common method is direct combustion of biomass material such as agriculture waste, solid waste, medical waste etc. has low efficiency and a high environmental impact, due to the release of particulates matter and various unburned hydrocarbons. Gasification of biomass is an attractive technology for power generation. The use of biomass gasification process is a key element in an advanced gas turbine combined cycle system (Deshmukh et al. 2013). In the last few years, many researchers have focused on biomass gasification

---

---

using a gas turbine, steam turbine combined cycle plant with integral biomass gasifier. Jurado et al. (2003) described modelling of combined cycle power plant using the waste material gasification of olive. Their results have been found of special importance for biomass fuelled gas turbine cogeneration technology. Kilmantos et al. (2009) investigated the air-blown gasification combined cycle based on biomass fuelled gas turbine and reported that a thermodynamic efficiency of more than 40% can be achieved by avoiding the exergetic losses in a pressurized high temperature condition combustion chamber. Bhattacharya et al. (2011) conducted a thermodynamic analysis of biomass integrated gasification combined cycle considering the combustion of supplementary biomass fuel using the oxygen available in gas turbine exhaust. Their results showed that supplementary firing of the biomass increases the plant efficiencies of a biomass integrated gasification combined cycle (BIGCC) plant till the optimum level of degree of firing. Srinivas et al. (2012) predicted the thermal performance of a biomass based integrated gasification combined cycle (IGCC) plant and examined the effects of gasifier conditions on the efficiency and power generation capacity of the plant as well as their effect on NO<sub>x</sub> and CO<sub>2</sub> emissions.

From the above reported investigation it is noted that all biomass materials used for combined power cycle generation have been gasified at ambient conditions. It is also seen that a considerable amount of heat is available at the exit of turbine of organic Rankine cycle, and very limited efforts have been made to recover this heat. In view of the above, a comprehensive thermodynamic analysis is conducted to observe the effect of change in biomass material and employment of ejectors between the steam turbine and condenser as well as in between refrigerant turbine and its condenser on first and second – law efficiencies of triple power cycle. Few investigations based on second – law analysis have already been conducted in the past for combined power and ejector refrigeration cycle (Sankarlal and Mani 2007; Dai et al. 2009; Khaliq 2015; Khalid et al. 2015). Recently, Habibzadeh et al. (2013) investigated the performance of the cycle operated on various refrigerants and found that R-601a has the highest thermal efficiency and lowest total exergy destruction under given operating conditions. They further observed that when the evaporation temperature increases the ejector entrainment ratio decreases while the total exergy destruction increases. Li et al. (2013) introduced double organic Rankine cycle based on the ORC. Parvez (2016) also proposed combined power and refrigeration cycle, which combines the Rankine cycle and the double-ejector refrigeration cycle. The results show that both the efficiencies increase with the employment of ejectors is 6.3% and 3.15% as compared to combined power cycle. The main objective of this paper is to examine, from an energetic and exergetic point of view, the possibilities and advantages of biomass fuelled triple power and ejector refrigeration cogeneration cycle concept. The performance of a combined production of power and refrigeration system along with its each effect was evaluated by using energy and exergy analysis to identifying the process efficiencies and their losses.

---

---

## 2.0 SYSTEM DESCRIPTION AND ASSUMPTION

The biomass is fed to the gasifier at ambient condition at 3, where syngas is produced in the presence of compressed air and superheat steam at state 2 and 4 as shown in Figure 1. The syngas produced in the gasifier after passing through a gas clean up unit goes to combustion chamber at 5. The syngas burned in the combustion chamber in the presence of compressed air, and the combustion products at 6 goes to gas turbine where they expand and produce power and exhaust gases of gas turbine at 7 enters HRSG where steam is generated. The superheat steam at 'a', goes to steam turbine for additional power production. Saturated steam at the exit of steam turbine at 'b' goes to the ejector for power production then goes to condenser where it gets condensed. The condensed liquid pumped back to HRSG. The stack gases at state 8 are routed through the evaporator where heat transfer occurs between the exhaust stream and the organic working fluid. The heated organic vapor is then enters in the turbine at 11 and just before final expansion, refrigerant vapor is extracted and enters to the ejector at 12 where it mixes with the secondary stream in the mixing chamber at 18 and produced refrigeration in the evaporator of ejector. Heat is rejected to the ambient in the condenser, and the cooled working fluid is divided into two streams one part throttles in the expansion valve for the ejector evaporator and rest of it pumped back to the HRVG. Stack gases at the exit of the HRVG discharged to the ambient at 9.

The following assumptions have been made for the analysis of the cycle (Srinivas 2009; Dai et al. 2009).

1. Air is admitted to the compressor at atmospheric conditions ( $p_0=1.013$  bar,  $T_0=298$  K).
2. Complete combustion takes place in combustion chamber.
3. The quantity of steam and fuel in gasification are taken to be as same.
4. Air fuel ratio (AFR) in the gasifier is assumed to be equal to 0.5.
5. The flow inside the ejector is in steady state and one-dimensional.
6. Velocities of streams at the inlet and outlet of the ejector could be negligible.
7. Mixing process in the mixing chamber of ejector occurs at constant pressure and complies with the conservation of energy and momentum.

## 3.0 ENERGY AND EXERGY ANALYSIS OF A COMBINED POWER AND EJECTOR REFRIGERATION CYCLE

In this system the following equations are used to calculate the absolute entropy of the species 'i' at various points reported by Moran and Shapiro (2007)

$$\bar{s}_i(T, p) = \bar{s}_i^0(T_0, p_0) + \int_{T_0}^T \frac{\bar{C}_{p_i}(T)}{T} dT - \bar{R} \ln \left( \frac{y_i p}{p_0} \right) \quad (1)$$

where,  $\bar{s}_i^0(T_0, p_0)$  is the absolute entropy of a species 'i' in kJ/kmol K,  $\bar{C}_{p_i}$  is the specific heat of a species 'i' at a given temperature (T) in kJ/kmol K, and  $y_i$  is the mole fraction of species 'i' in the mixture.

$$\bar{s}_{mix}(T, p) = \sum_{i=1}^{i=n} y_i \bar{s}_i(T, p) \quad (2)$$

$$\frac{\bar{C}_{p_i}(T)}{\bar{R}} = \alpha + \beta T + \gamma T^2 + \delta T^3 + \varepsilon T^4 \quad (3)$$

$$\bar{C}_{p,mix} = \sum_{i=1}^{i=n} y_i \bar{C}_{p_i} \quad (4)$$

The formulation and assumption of entrainment ratio is based on mass, momentum and energy equations which is recently developed by Dai et al. (2009)

$$\mu = \sqrt{\eta_n \eta_m \eta_d (h_{pf,n1} - h_{pf,n2,\dot{s}}) / (h_{mf,d,\dot{s}} - h_{mf,m})} - 1 \quad (5)$$

The efficiencies of nozzle, mixing chamber, and diffuser are reported in Table 2 and the required enthalpy values are taken from REFPROP 6.01(1998).

The energy conservation equation for the adiabatic and steady primary flow is given as

$$\dot{m}_{pf} h_{pf,n2} + \frac{\dot{m}_{pf} u_{pf,n2}^2}{2} = \dot{m}_{pf} h_{pf,n1} + \frac{\dot{m}_{pf} u_{pf,n1}^2}{2} \quad (6)$$

The nozzle efficiency may be calculated as

$$\eta_n = \frac{h_{pf,n1} - h_{pf,n2}}{h_{pf,n1} - h_{pf,n2,\dot{s}}} \quad (7)$$

In the mixing section, the momentum conservation equation is given as

$$\dot{m}_{pf} u_{pf,n2} + \dot{m}_{sf} u_{sf,n2} = (\dot{m}_{pf} + \dot{m}_{sf}) u_{mf,m,\dot{s}} \quad (8)$$

In the diffuser section, the energy equation is given as

$$\frac{1}{2} (u_{mf,m}^2 - u_{mf,d,\dot{s}}^2) = h_{mf,d,\dot{s}} - h_{mf,m} \quad (9)$$

The diffuser efficiency is given as



$$\eta_d = \frac{h_{mf,d,s} - h_{mf,m}}{h_{mf,d} - h_{mf,m}} \quad (10)$$

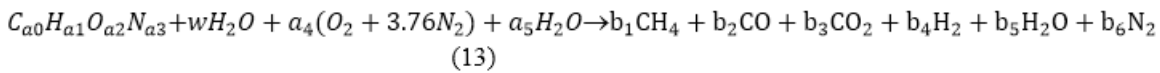
The compressor delivery pressure  $p_2$  is evaluated using the cycle pressure ratio ( $r_p$ ), which is fixed at 12 bar. The temperature of air at the exit of compressor is obtained by using the isentropic relation as

$$\frac{T_2}{T_1} = \left(\frac{p_2}{p_1}\right)^{\frac{\gamma-1}{\gamma c_p}} \quad (11)$$

The actual power input to the compressor of admitted air ( $W_c$ ) is calculated by using the relation

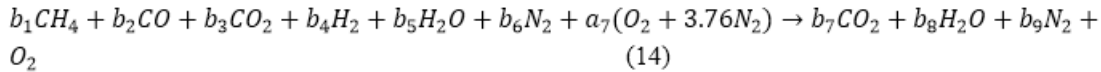
$$W_c = m_{air} \left[ \alpha_{air}(T_2 - T_1) + \frac{\beta_{air}}{2}(T_2^2 - T_1^2) + \frac{\gamma_{air}}{3}(T_2^3 - T_1^3) + \frac{\delta_{air}}{4}(T_2^4 - T_1^4) \right] \quad (12)$$

The general chemical formula for biomass feedstock is given by  $C_{a0}H_{a1}O_{a2}N_{a3}$ . The global gasification reaction in the biomass gasifier can be written as



The composition of biomass materials is reported in Table 1 and coefficient of syngas is given in Table 3.

The complete combustion equation for syngas in gas turbine combustion chamber with complete air is



In Eq. (14) ' $a_7$ ' is the amount of air to be supplied into the GTCC. The calorific value of synthetic gas at a given combustion outlet temperature may be given as

$$\sum_R (\bar{h}_f^0 + \Delta \bar{h}) + \bar{Q}_{cv} = \sum_P (\bar{h}_f^0 + \Delta \bar{h}) \quad (15)$$

The isentropic efficiency of gas turbine and pressure ratio across the turbine as

$$W_{GT} = m_{mix} \left[ \alpha_{mix}(T_6 - T_7) + \frac{\beta_{mix}}{2}(T_6^2 - T_7^2) + \frac{\gamma_{mix}}{3}(T_6^3 - T_7^3) + \frac{\delta_{mix}}{4}(T_6^4 - T_7^4) \right] \quad (16)$$

$$\eta_I = \frac{W_{GT} + \dot{W}_{ST} + \dot{W}_{RT} - \dot{W}_{AC} - \dot{W}_{P1} - \dot{W}_{P2} + \dot{Q}_E + \dot{Q}_R}{\dot{m}_f LHV} \quad (17)$$

where  $m_f$  is the mass flow rate of fuel consumed

$$\eta_{II} = \frac{W_{GT} + \dot{W}_{ST} + \dot{W}_{RT} - \dot{W}_{AC} - \dot{W}_{P1} - \dot{W}_{P2} + \dot{E}_E + \dot{E}_R}{\dot{E}_{fuel,in}} \quad (18)$$

$$\dot{E}_E = \dot{Q}_E \left( \frac{T_0 - T_E}{T_0} \right) \quad (19)$$

where  $\dot{E}_{fuel,in}$  is the exergy of fuel and  $\dot{E}_E$  is the amount of exergy associated with the refrigeration capacity ( $\dot{Q}_E$ ) of the ejector evaporator.

#### 4.0 RESULTS AND DISCUSSION

The parametric study is carried out to identify the effect of some influenced parameters on the performance of the integrated gasification combustion chamber and double-ejector refrigeration cycle. Following parameters have been chosen in the typical range of its operation: gas turbine inlet temperature (1000 °C–1200°C) and turbine inlet pressure (30 bar to 70 bar), whereas values of other parameters are kept constant at the level of base case values. Manure and solid waste were the biomass materials taken into consideration due to their significant variation of calorific values. The thermodynamic properties of R141b of ejector refrigeration cycle were calculated by REFPROP 6.01 (1998).

Figures 2-3 shows the energetic and exergetic efficiencies of biomass gasification based on triple power cycle with and without considering the ejector refrigeration system with the change in turbine inlet temperature. In general, exergetic efficiencies of both triple power and combined power and ejector refrigeration cycles are slightly lower than their energetic efficiencies. This is due to the fact that the chemical exergy of fuel (biomass) which is considered as the input in exergy analysis is slightly higher than the calorific value of the fuel which is considered as the input in the energy analysis. On comparing the performance of triple power cycle with and without ejector refrigeration system, energetic efficiency has improved considerably while exergetic efficiency of the triple power cycle increased marginally with the employment of ejector refrigeration system. This is due to the reason that amount of exergy associated with the refrigeration capacity of the ejector is considerably lower than the energy of the refrigeration capacity. In general, it is observed that employment of ejector in triple power cycle enhances its energetic efficiency in the range (8.5% - 8.75%) for both the biomass materials considered. On the other hand second – law efficiency of the same cycle increased between (5.5%-5.9%) due to the reasons explained above. It also shown that energetic and exergetic efficiencies of manure fuel is higher than the energetic and exergetic efficiencies of triple power cycle of solid waste fuel triple power cycle. This is because the energy and exergy contents of solid waste fuelled are considerably higher than the energy and exergy contents of manure fuelled.

Figures 4-5 shows the variation of energetic and exergetic efficiencies of triple power cycle with the

---

---

change in steam turbine inlet pressure. It is found that both energetic and exergetic efficiencies decrease slightly with the increase in steam turbine inlet pressure. The reason for this is that increase in turbine inlet pressure results in lower mass flow rate of steam produced in the heat recovery steam generation which in turn reduces the steam turbine output and hence decreases the overall efficiency of the cycle. Since the contribution of gas turbine towards overall generation is much higher and its three times larger than the contribution of the steam turbine, and change in steam turbine pressure only affects the steam turbine output not the gas turbine output, therefore energetic efficiency of triple power cycle slightly drops with the increase in steam turbine inlet pressure. For the similar reasons exergetic efficiency also drops slightly with the same. An effect of ejector employment in triple power cycle for different steam turbine inlet pressures on both energetic and exergetic efficiencies is also shown in the above figures. It is further observed energetic and exergetic efficiencies of triple power cycle are showing the trend similar with respect to steam turbine inlet pressure. Due to the higher energy and exergy contents of solid waste fuel are higher than the energy and exergy contents of manure fuelled triple power cycle.

## 5. CONCLUSION

The biomass based integrated gasification combined cycle plant with ejector refrigeration cycle is examined with gasifier condition. A novel combined power and ejector refrigeration is proposed, which combines the Rankine cycle and ejector refrigeration cycle. Energetic and exergetic analyses are performed to evaluate the thermodynamic improvement for this newly cycle. From the above discussion it can be concluded that:

- Both energetic and exergetic efficiencies of combined power and ejector refrigeration cycle increase with the increase in gas turbine inlet temperature.
- There is on average 8.75% gain in energetic efficiency and 5.9% gain in exergetic efficiency of triple power cycle when ejectors are employed.
- Slight variation in both energetic and exergetic efficiencies were obtained when the biomass fuels are changed from manure to solid waste is observed.
- Both energetic and exergetic efficiencies of combined power and ejector refrigeration cycle slightly decrease when steam turbine inlet pressure increased from 30 to 70 bar.
- Manure fuelled cogeneration provides higher energetic and exergetic than Solid waste fuelled cycle due to the considerable difference in their energy and exergy contents.

Results presented here could be used for simulation and design of biomass gasification and combustion of syngas for power generation. Effective exploitation of biomass and waste heat recovery can be

---

---

achieved with the employment of proposed cogeneration cycle.

## Nomenclature

C	compressor, Carbon
C1	steam condenser
C2	refrigerant condenser
$\dot{E}_{fuel,in}$	<u>exergy</u> of fuel (kW)
$\dot{E}_R$	<u>exergy</u> of refrigeration effect (kW)
HRVG	heat recovery vapor generator
$\Delta\bar{h}$	<u>change</u> in enthalpy of a species or mixture from ambient state to given state (kJ/ <u>kmol</u> )
$\bar{h}_f^0$	<u>enthalpy</u> of formation of species of a mixture at ambient conditions (kJ/ <u>kmol</u> )
$\dot{m}$	<u>mass</u> flow rate (kg/s)
$\dot{m}_f$	mass flow rate of fuel consumed (kg/s)
$\dot{m}_{vapor}$	mass flow rate of refrigerant (R-141b) vapor in ejector refrigerant cycle (kg/s)
P	product
$\bar{Q}_{cv}$	<u>calorific</u> value (kJ/kmol)
$\dot{Q}_E$	refrigeration capacity of the ejector evaporator (kW)
$\dot{Q}_R$	refrigeration effect in refrigerator (kW)
R	reactant
$\bar{R}$	<u>universal</u> gas constant (kJ/ <u>kmol</u> K)
RT	refrigerant turbine
S	specific entropy (kJ/kg- K)
TV	throttling valve
$u$	velocity (m/s)
$\eta_I$	<u>first</u> law efficiency
$\eta_{II}$	<u>second</u> law efficiency
$\mu$	<u>entrainment</u> ratio in the ejector

---

---

## Suffix

<u>a-h</u>	state points of the steam cycle
<u>bmf</u>	biomass fuel
C	compressor
<u>d a f</u>	<u>dry</u> ash free
F	formation, fuel
<u>d</u>	diffuser
<u>n</u>	nozzle
<u>m</u>	mixing chamber
<u>pf</u>	primary flow
<u>sf</u>	secondary flow
<u>n1</u>	inlet of nozzle
<u>n2</u>	outlet of nozzle
<u>s</u>	<u>isentropic</u>
1-18	state numbers of the combined power and refrigeration cycle

## REFERENCES

- Bhattacharya A, Manna D, Paul B, Data A (2011) Biomass integrated gasification combined cycle power generation with supplementary biomass firing: energy and exergy based performance analysis. *Energy* 36(5): 2599-2610.
- Deshmukh, Ranjit AJ, Charles C, Dan K (2013) Thermal gasification or direct combustion? Comparison of advanced cogeneration systems in the sugarcane industry. *Biomass and Bioenergy* 55: 163-174.
- Dai Y, Wang J and Gao L (2009) Exergy analysis, parametric analysis and optimization for a novel combined power and ejector refrigeration cycle. *Applied Thermal Engineering* 29: 1983-1990.
- Habibzadeh A, Rashidi MM and Galanis N (2013) Analysis of a combined power and ejector-refrigeration cycle using low temperature heat. *Energy Conversion and Management* 65: 381-391.
- Jurado F, Cano A, Carpio J (2003) Modeling of combined cycle power plants using biomass. *Renewable Energy* 28, 743-753
- Khalid F, Dincer I and Rosen MA (2015) Energy and exergy analyses of a solar-biomass integrated cycle for multigeneration. *Solar Energy* 112: 290-299.
- Khaliq A (2015) Performance analysis of a waste heat powered thermodynamic cycle for multieffect refrigeration. *International Journal of Energy Research* 39:529-542.
- Kilmantos P, Koukouzas N, katsiadakis A, kakaras E (2009) Air-blown biomass gasification combined cycles (BGCC): system analysis and economic assessment. *Energy* 34: 708-714.
- Li X, Li X, Zhang Q (2013) The first and second law analysis on an organic Rankine cycle with ejector. *Solar Energy* 93: 100-108.
- Moran MJ and Shapiro HN (2007) *Fundamentals of engineering thermodynamics*. 6<sup>th</sup> Edition, Johan Wiley & Sons USA.

NIST Standard Reference Database 23, NIST Thermodynamic and Transport Properties of Refrigerants and Refrigerants Mixtures REFPROP, Version 6.01, 1998.

Parvez M (2016) First and second law analyses of syngas fuelled novel combined power and double – ejector refrigeration cycle. *Biofuels* DOI: 10.1080/17597269.2016.1215067.

Sankarlal T, Mani A (2007) Experimental investigation on ejector refrigeration system with ammonia. *Renewable Energy* 32: 1403-1413.

Srinivas T, Gupta AVSSKS, Reddy BV. Thermodynamic equilibrium model and exergy analysis of a biomass gasifier. *Journal of Energy Resources Technology* 2009; 131(03):1801-1-7.

Srinivas T, Reddy B.V and Gupta A.V.S.S.K.S (2012). Thermal performance prediction of a biomass based integrated gasification combined cycle plant. *Journal of Energy Resources Technology* Vol. 134/ 021002-1-9.

**Table1. Thermo-chemical properties of biomass materials**

Property	Units	Manure	Solid Waste
C	Wt% daf	50.20	51.03
H	Wt% daf	6.50	6.77
O	Wt% daf	34.60	39.17
N	Wt% daf	5.20	2.64
Lower Heating Value	kJ/kg,daf	25203.85	25021.51
Moisture Content	Wt%	13.00	16.00
Ash	Wt%	0.90	5.00
Exergy Ratio		1.01	1.04

**Table2. Properties and operating variables for the analysis of the proposed Combined power and refrigeration cooling cycle configuration**

<b>Properties of Ambient Air</b>	
Pressure (bar)	1.013
Temperature (K)	298
<b>Composition (by volume)</b>	
Nitrogen	79%
Oxygen	21%
<b>Operating Parameters</b>	
Isentropic efficiency of compressor ( $\eta_{c,isen}$ )	85%
Isentropic efficiency of gas turbine ( $\eta_{gt,isen}$ )	85%
Isentropic efficiency of steam turbine ( $\eta_{st,isen}$ )	85%
Pressure drop across the gasifier ( $\Delta P_G$ )	5%
Pressure drop across the combustion chamber ( $\Delta P_{CC}$ )	3%

Pressure drop across the HRSG ( $\Delta P_{HRSG}$ )	2%
Compressor pressure ratio ( $r_p$ ) bar	12 (fixed)
Turbine inlet temperature TIT ( $^{\circ}C$ )	1000–1200 (range)
Condenser pressure (bar)	0.06
Pinch point temperature	30 K (fixed)
Approach temperature	15 $^{\circ}C$
Steam turbine inlet pressure (bar)	30 – 70 (range)
Refrigerant turbine isentropic efficiency	80%
ORC pump isentropic efficiency	85%
Nozzle efficiency	90%
Mixing chamber efficiency	85%
Diffuser efficiency	85%

**Table3. Composition of synthetic gas produced after gasification and exhaust gas after composition for one kmol of biomass at pressure ratio ( $r_p=12$ )**

Constituent	Manure	Solid Waste
	Concentration (kmol)	Concentration (kmol)
<b>Syngas</b>		
CH <sub>4</sub>	b1=0.17	b1=0.16
CO	b2=0.47	b2=0.52
CO <sub>2</sub>	b3=0.33	b3=0.32
H <sub>2</sub>	b4=0.77	b4=0.84
H <sub>2</sub> O	b5=0.89	b5=0.94
N <sub>2</sub>	b6=0.47	b6=0.44
<b>Combustion Product</b>		
CO <sub>2</sub>	b7=1	b7=1
H <sub>2</sub> O	b8=2	b8=2.1
N <sub>2</sub>	b9=6.251	b9=6.08
O <sub>2</sub>	0.5475	0.5
a <sub>7</sub>	1.5375	1.5

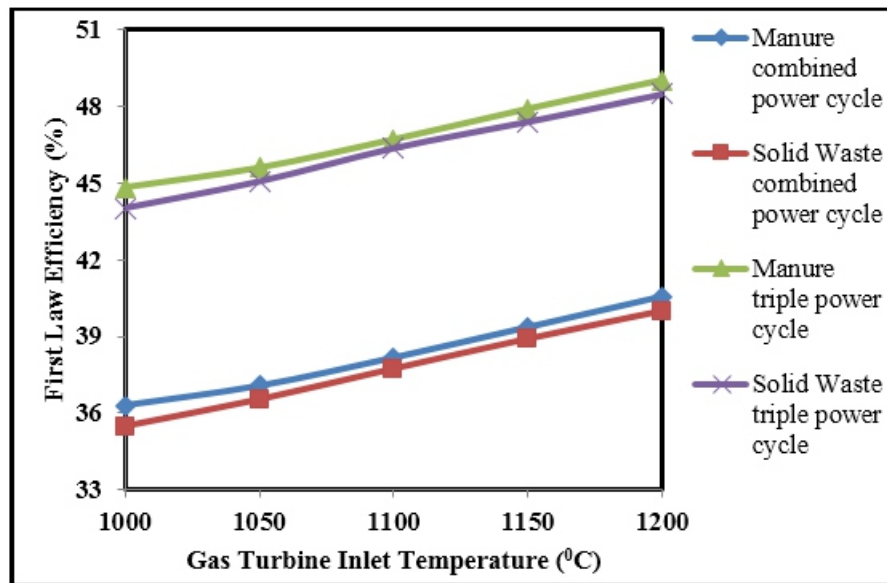


Fig.2 Variation of energetic efficiency of combined and triple power cycle with gas turbine inlet temperature at ( $r_{10}=12$ )

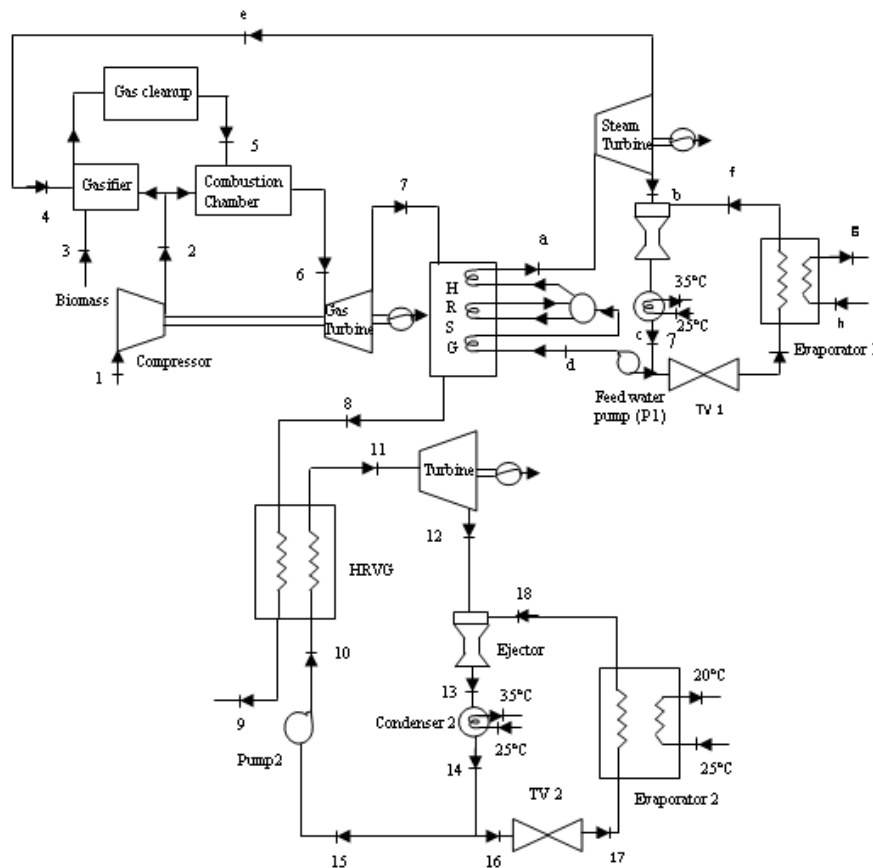


Fig.1 Schematic diagram of biomass fuelled combined power and refrigeration cooling cycle



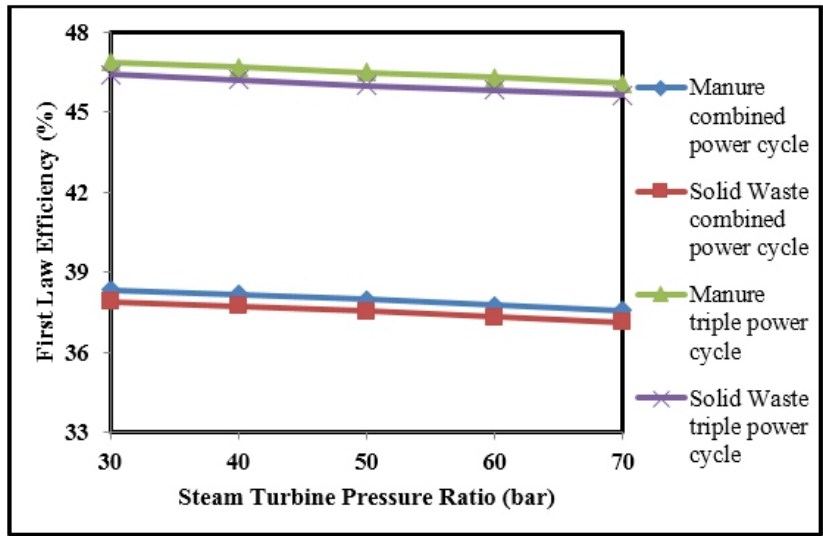


Fig.4 Variation of energetic efficiency of combined and triple power cycle with steam turbine inlet pressure at (TIT=1100 0C)

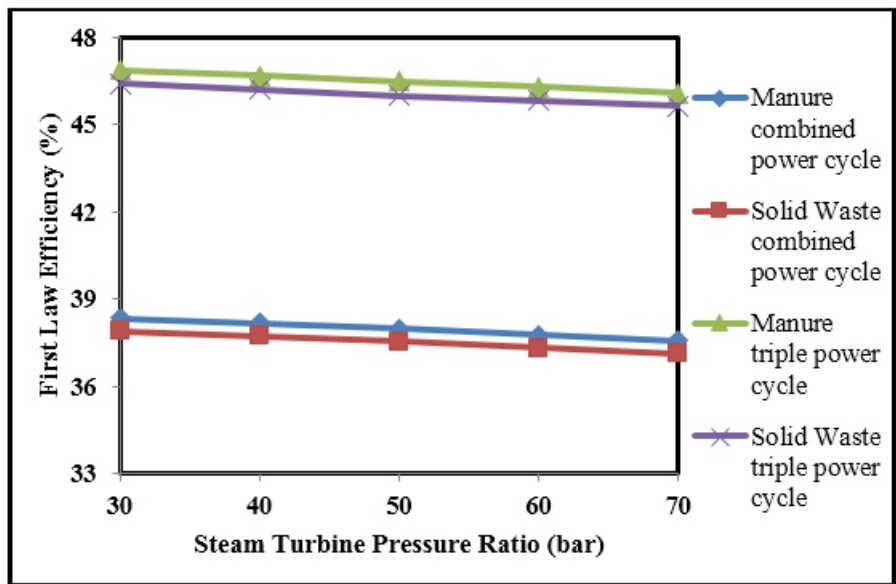


Fig.5 Variation of energetic efficiency of combined and triple power cycle with steam turbine inlet pressure at (TIT=1100 0C)

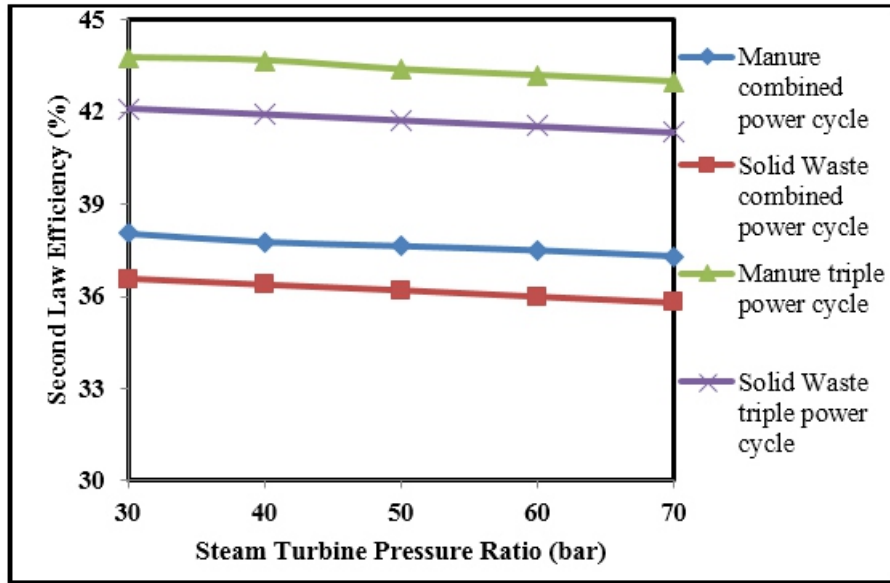


Fig.5 Variation of exergetic efficiency of combined and triple power cycle with steam turbine inlet pressure at (TIT=1100 °C)

---

---

## Refrigeration using Green Secondary Refrigerant (Ice Slurries) - Some Studies on Ice Slurries and Scraped Surface Ice Slurry Generator

**Dr. Rajinder Singh<sup>1</sup>**

<sup>1</sup>Senior Faculty, Pusa Institute of Technology, Pusa, New Delhi  
Email ID:rajindersingh1102@gmail.com



### **ABSTRACT**

A scraped surface ice slurry generator has been designed, developed and fabricated with a focus on collection of experimental data related to ice crystallization mechanism in the microscopic scale, heat transfer and fluid mechanics involving agitation and phase change in the macro scale for the ice slurry (green secondary refrigerant) production. Experimental study shows that at different concentrations of antifreezes (PG and MEG), initially the freezing temperature reduces sharply with time (stage 1), then there is sudden rise in temperature for very short duration of time (stage 2) and finally it slowly reduces whereas freezing temperature reduces with increase in antifreeze mass fraction. Freezing temperature is inversely proportional to antifreeze mass fraction.

*Keywords—ice slurry, depressants, scraped surface generator, performance study.*

### **1. INTRODUCTION**

Ice slurry has a great potential for the future due to wide range of industrial applications varying from comfort cooling and commercial refrigeration to industrial production processes medicine and in the milk production where high peak loads are to be adjusted. Ozone depletion and global warming forced the refrigeration and air-conditioning industry to reexamine the utility of 'old' and industrially viable refrigerants (such as methane, ethane, propane etc) to be attractive, because of their zero ODPs. In the 1930s these have been replaced by new chemical compounds, namely CFCs and HCFCs. The prime advantages of these synthetic materials were nontoxicity and nonflammability, whereas the disadvantage is their impact on environment. Besides this the leakage of toxic or/and flammable 'old' refrigerants require leakage free systems or as an alternative a secondary circuit with a special cooling fluid for heat abstraction. It was precisely this development, mainly responsible for the utility of the ice slurry technology in the present scenario.

Recent developments in the ice slurry generator technology and advanced design concepts have made this technology a industrially viable alternative to existing conventional secondary refrigeration

---

---

systems. Presently, the major research work for development of ice slurry generator has taken place only in developed countries due to very high fixed cost. The scraped surface ice slurry generator is commercially the most technologically developed and widely accepted ice slurry generation process over the last two decades. From the literature review it is clear that the basic understanding of the governing ice slurry crystallization mechanism is rather limited and is still speculative. Further, at present the design of ice slurry generation system are purely in the hands of ice slurry manufacturer who keep detailed operating data proprietary. Therefore there is an urgent need for better understanding of basic crystallization and heat transfer mechanisms to optimize and develop relatively compact, efficient and less costly ice slurry generators.

Ice slurry is a phase-changing secondary fluid consisting of both a liquid state fraction and a solid-state fraction. Depending on the type of additive and additive concentration, the operating temperature for ice slurry can be chosen from 0 to at least  $-35^{\circ}\text{C}$  [1,2]. Beyond the advantages of the traditional indirect systems for lowering the emissions of refrigerants and refrigeration plants, ice slurry is a more efficient secondary fluid than single-phase fluids. Using ice slurry with accumulation increases the possibility to build indirect systems without increasing the energy consumption.

The time required for ice to cover the unscraped cooling surface; the thermal response of the supercooled solution at the onset of phase change; the heat transfer coefficient on the scraped surface with/without phase change, and the growth kinetics of ice film spreading along the cooling surface was studied by Frank et al. [4]. Continuous heat extraction is important for the process of freeze concentration of aqueous solutions, in which water is removed as solid ice. Three typical heat-transfer patterns were identified during the process of freeze concentration in an SSHE. These correspond to the stages of chilling, nucleation, and crystallization, respectively [5]. Heat transfer is an unsteady process in the initial period of ice nucleation or phase transition from aqueous solution. Using the Laplace and inverse transform, and incorporating the initial condition of ice nucleation, an analytical solution of this model is obtained by Frank et al. [6].

Heat transfer phenomena in two types of eutectic crystallizers have been analyzed by Vaessen et al. [7]. Application of the analytical solution leads to the predictions of the growth rate of ice films on different materials, and the temperature distribution in the solid slab right underneath the growing front of the ice film [8]. For ice slurries to become more widely accepted, however, more engineering information is required on fluid flow and heat transfer characteristics. In a practical application, for a given thermal load this would lead to greater than 60% reduction in flow rate and pressure drop compared to chilled water cooling systems [9]. In recent years, a lot of important work has been carried out in order to gather

---

---

knowledge of the fundamental behaviour of ice slurry in piping systems and heat exchangers [10].

An experimental study was carried out on a scraped surface heat exchanger used for freezing of water–ethanol mixture and aqueous sucrose solution. The influence of various parameters on heat transfer intensity was established [11]. A performance assessment of four main types of ice storage techniques for space cooling purposes, is conducted by David and Dincer [12]. The results show that energy analyses alone do not provide much useful insight into system behavior, since the vast majority of losses in all processes are a result of entropy generation which results from system irreversibility.

A successful way to enhance the thermal capacity of secondary fluid systems is by incorporating microencapsulated phase change material (MPCM) slurry. However, a full understanding of the physical properties and heat transfer characteristics of MPCM slurry in the 2–8 0C range still is lacking. The experimental data show that MPCM slurry can provide considerable heat capacity in heat transfer applications [13]. The characteristics of three different principles of pumps-centrifugal, side-channel and screw were investigated [14]. The heat transfer coefficient and the power consumption of a laboratory scraped-surface heat exchanger (SSHE) were measured when it was used for freezing a 10 wt. % sugar solution. Experimental results show that the heat transfer coefficient with phase change (ice formation) was about three to five times greater than that without phase change [15]. Effect of poly vinyl alcohol (PVA) in inhibiting an increase in ice crystal size in isothermal ice slurries was investigated, and then compared with the effect of an antifreeze protein (AFP), NaCl [16].

A new type of sensor for in-line measurements of antifreeze mass fraction in aqueous solutions is described by Vincet et al. [17]. Latent heat of fusion of ice in aqueous solutions was measured to understand latent heat of fusion of ice slurries. Propylene glycol, ethylene glycol, ethanol, NaCl and NaNO<sub>3</sub> solutions were used as aqueous solutions. [18]. The study by Matsumotoa [19] focuses on an emulsion as a new thermal storage material for ice storage. This study by Guilpart et al. [20] compares the performance of several commonly used organic and inorganic ice slurry secondary refrigerants. For ice slurry calculations and modeling, it is important that they are performed with accurate thermo physical property values of the aqueous solution and of ice. For ice slurry applications there is a need for accurate freezing point data and for more basic thermo physical property data at low concentrations [21]

In the present experimental study 'scraped surface ice slurry generator' of 5 litre capacity has been designed, developed and fabricated with a focus on collection of experimental data related to ice crystallization mechanism in the microscopic scale, and heat transfer and fluid mechanics involving agitation and phase change in the macro scale for the ice slurry production [15]. The main components

---

---

of ice slurry circuit are: Scraped surface ice slurry generator with a scraper, condensing unit, pump and a storage tank. The scraped surface ice slurry generator consists of a circular shell and coil type heat exchanger cooled by an evaporating refrigerant flowing in a spiral shape coil around the outer shell side. The inner cooled surface of the shell is scraped by spring loaded rotating blades to prevent crystal depositions. This scraping action is required to prevent the formation of an ice layer on the ice generator walls. Turbulence is mechanically induced into the ice slurry flow by the action of the rotating scraper blades mounted in the centre of the generator, thus greatly enhances the heat transfer rates and thus facilitating the production of a homogeneous ice slurry mixture. This unit supplies the refrigerant to the coil of the ice slurry generator (referred as evaporator in the refrigeration cycle) where evaporating refrigerant at lower pressure withdraws heat from the binary solution which is finally converted into ice slurry. Experimental studies have been performed using water and various depressants such as propylene glycol, methyl alcohol, ethyl alcohol in different proportions. Performance studies have been conducted for wide range of operating variables.

## 2. RESULTS AND DISCUSSIONS

In continuation to our previous work [22] 'Development of Scraped Surface Ice Slurry Generator' experiments were carried out. The aqueous solution of antifreezes, Propylene Glycol (PG) and Mono Ethylene Glycol (MEG) with water at different weight percentages 10%, 20% and 30% of antifreezes and 90%, 80% and 70% of water respectively were subjected to the freezing process. The coolant temperatures were measured with RTD. Recorded temperatures of aqueous solution of Antifreezes (PG and MEG) at various concentrations are plotted (Figs. 1,2,3,4,5 and 6) with respect to freezing time of ice slurry for PG and MEG, respectively. With antifreeze PG, the lowest ice slurry temperatures achieved are  $-2.9^{\circ}\text{C}$ ,  $-6.4^{\circ}\text{C}$  and  $-11.0^{\circ}\text{C}$  at 10%, 20% and 30% concentrations respectively, whereas with antifreeze MEG, lowest ice slurry temperatures achieved are  $-3.4^{\circ}\text{C}$ ,  $-7.1^{\circ}\text{C}$  and  $-11.9^{\circ}\text{C}$  at 10%, 20% and 30% concentrations respectively. Freezing temperatures vs. antifreeze mass fraction is shown in Fig. 7. A photograph of ice slurry formation is shown in Fig. 8.

Historical time curves (recorded temperatures of aqueous solution of antifreezes, refrigerant temperatures at evaporator inlet and outlet, refrigerant temperatures at condenser inlet and outlet, ice slurry temperatures at different concentrations), and freezing temperatures vs. antifreeze mass fraction are plotted. Recorded temperatures of aqueous solution of antifreezes, refrigerant temperatures at evaporator inlet and outlet, refrigerant temperatures at condenser inlet and outlet at different concentrations are plotted (Figs. 1 to 3 for PG and Figures 4 to 6 for MEG) with respect to freezing time. From the present experimental ice slurry generation data it can be observed that ice slurry generation

---

---

process can be divided into three stages- cool down or chilling period, nucleation or unstable ice slurry generation period and stable ice generation period. The first stage (cool down period) starts  $t_0$  to  $t_1$ , where  $t_0$  is the starting time of the experiment and  $t_1$  is the time at the end of the chilling period which is the on-set of the super-cooling phenomenon. During the chilling period volumetric ice concentration is zero. As observed in Figs 1 to 3, the freezing temperature reduces with increase in antifreeze mass fraction for PG solution initially chilled continuously without phase change in stage 1. First phase time duration is 1500, 1600 and 2000 seconds respectively for 10%, 20% and 30% concentration of PG. Similar trend was observed for MEG (Figures 4 to 6) but first phase time duration was relatively higher as compared to PG. During this stage the average evaporator temperature decreases sharply which causes increase in the refrigeration capacity and compressor work. Therefore, the condenser inlet temperature increases due to higher heat rejection quantity. Volumetric ice concentration is zero during the chilling period. During this stage the average evaporator temperature decreases sharply due to unsteady state nature of heat transfer through the shell of ice slurry generator. The outlet temperature of evaporator outlet is stabilized when the nucleation period starts.

The second stage (nucleation period) starts from  $t_1$  to  $t_2$ , where the ice seeds after the super cooling phenomenon is observed and the volumetric ice concentration increases till its maximum value at the end of this period (at  $t_2$ ). In stage 2, nucleation of ice particles occurs and it is characterized by 0.5 to 1<sup>o</sup>C jump in temperature of the process fluid due to the release of the fusion heat of ice. Finally the third stage (ice slurry generation period) starts from  $t_2$  to the end of the experiment, at  $t_r$ . During this stage the ice concentration is maintained constant at its maximum value. During stage 3 the heat transfer is affected by the release of the latent heat of water freezing.

Freezing temperatures vs. antifreeze mass fraction is shown in Fig. 7. Here, freezing temperature is inversely proportional to antifreeze mass fraction. When water freezes out after the temperature of the liquid mixture has passed below the freezing point, the concentration of the additive increases in the liquid-phase. The increased additive concentration implies that the freezing point of the remaining liquid-phase is further lowered and in order to freeze out more ice the temperature of the mixture has to be further lowered below the current freezing point of the liquid. The result is that the fluid has a freezing range rather than a definitive freezing point. Thus by plotting the freezing point as a function of the additive concentration, one obtains a freezing point curve as a function of the additive mass concentration of different freezing point depressants (Fig. 7). Lowering of the temperature of the ice slurry is independent of the effect of the latent heat from the phase change, but dependent on the sensible heat of the mixture. Since it is the advantage of the latent heat in ice slurry that is desired, one desires a liquid mixture where the latent heat dominates. To minimize the influence of the sensible heat, a fluid



with a relatively low first derivative of the freezing point curve (flat freezing point curve) is to be preferred.

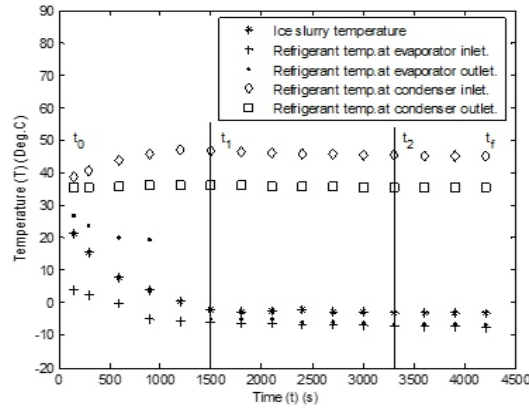


**Fig.1. Freezing temperature vs time for PG at 10 % concentration**

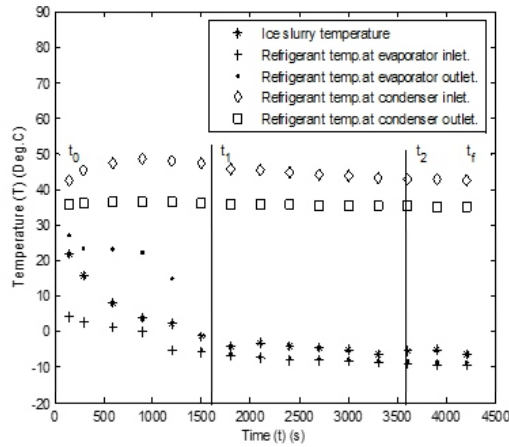


**Fig.2. Freezing temperature vs time for PG at 20 % concentration**

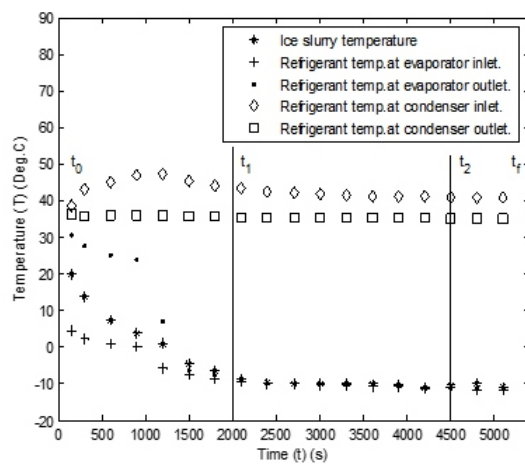


**Fig.3. Freezing temperature vs time for PG at 30 % concentration**



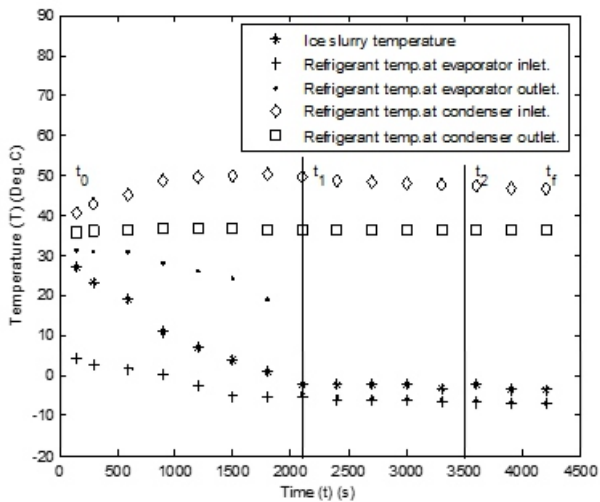


Fig.4. Freezing temperature vs time for MEG at 10 % concentration

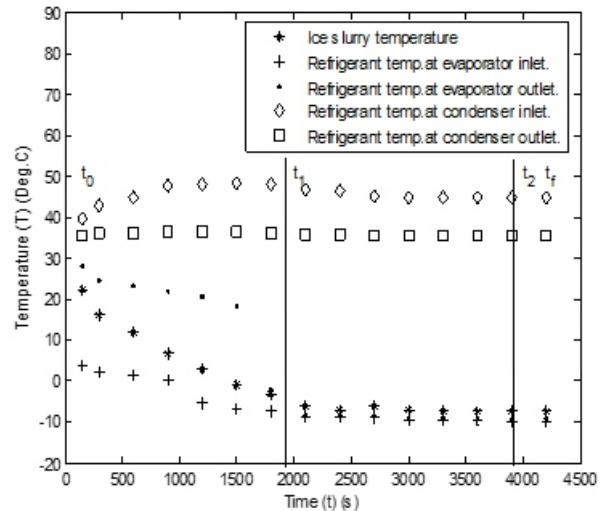


Fig.5. Freezing temperature vs time for MEG at 20 % concentration

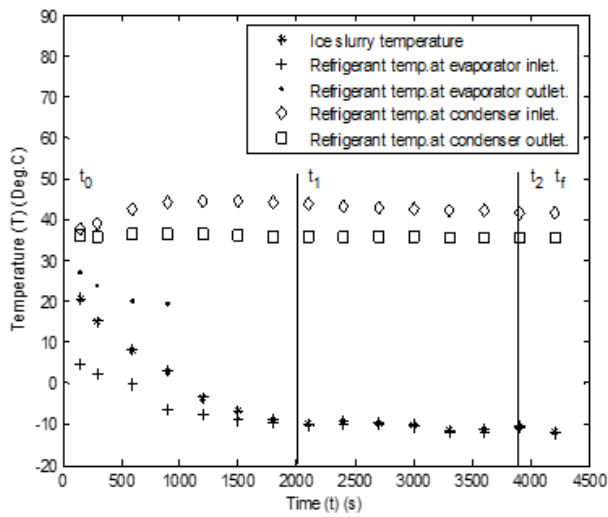


Fig.6. Freezing temperature vs time for MEG at 30 % concentration

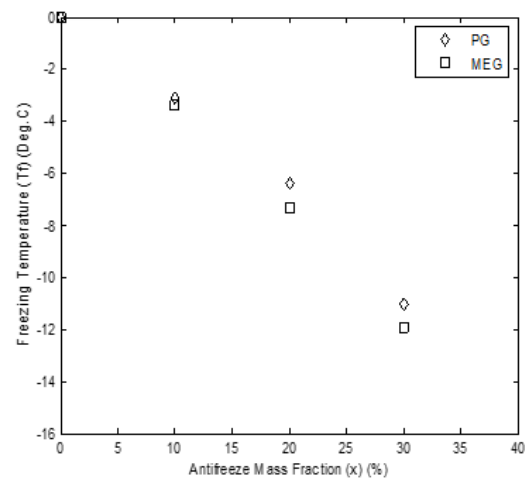


Fig.7. Freezing curve of water-PG and water- MEG mixture

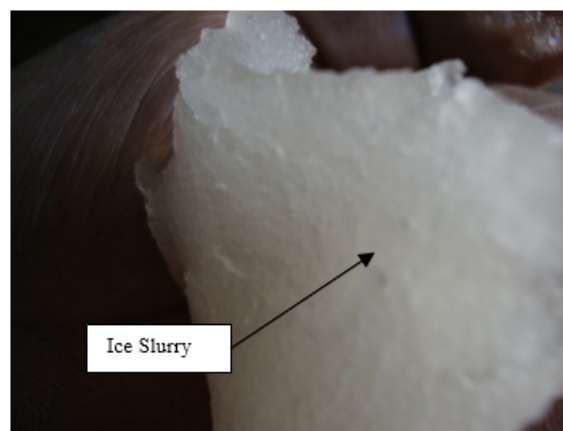


Fig. 8. Photograph of Ice Slurry of  $-11.9^{\circ}\text{C}$  formation in SSISG using MEG

---

### 3. CONCLUSIONS

From the present experimental data it can be concluded that at different concentrations of antifreezes (PG and MEG), initially the freezing temperature reduces with time (stage 1), then there is sudden rise in temperature for very short duration of time (stage 2) then reduces. It is observed that the freezing temperature reduces with increase in antifreeze mass fraction for PG and MEG solution initially chilled continuously without phase change in stage 1. In stage 2 of very short duration, nucleation of ice particles occurs and it is characterized by a distinct jump in temperature of the process fluid due to the release of the fusion heat of ice. During stage 3 the heat transfer is affected by the release of the latent heat of water freezing and freezing temperature is inversely proportional to antifreeze mass fraction [20, 24].

### 4. REFERENCES

- [1] Åke Melinder., *Thermophysical Properties of Aqueous Solutions Used as Secondary Working Fluids*, Doctoral Thesis, Division of Applied Thermodynamics and Refrigeration Dept. of Energy Technology School of Industrial Engineering and Management Royal Institute of Technology, KTH Stockholm, Sweden, 2007.
- [2] Cecilia Hägg., *Ice Slurry as Secondary Fluid in Refrigeration Systems Fundamentals and Applications in Supermarkets*, Licentiate Thesis, Stockholm, School of Industrial Engineering and Management Department of Energy Technology Division of Applied Thermodynamics and Refrigeration, 2005.
- [3] M. Kauffeld, M.J. Wang, V. Goldstein, K.E. Kasza, "Ice Slurry Applications", *International Journal of Refrigeration*, Vol. 33, 2010, pp.1491-1505.
- [4] Frank G.F. Qin a., Xiao Dong Chen , Kevin Free, "Freezing on subcooled surfaces, phenomena, modeling and applications", *International Journal of Heat and Mass Transfer*, Vol. 52, 2009, pp.1245–1253.
- [5] Frank G. F. Qin, Xiao Dong Chen, and Andrew B. Russell, "Heat Transfer at the Subcooled-Scraped Surface, with/without Phase Change", *AIChE Journal*, Vol. 49, No. 8, 2003, pp. 1947- 1955.
- [6] Frank G.F. Qin, Jian Chao Zhao , Andrew B. Russell , Xiao Dong Chen , John J. Chen , Lindsay Robertson, "Simulation and experiment of the unsteady heat transport in the onset time of nucleation and crystallization of ice from the subcooled solution", *International Journal of Heat and Mass Transfer*, Vol. 46, 2003, pp. 3221–3231.
- [7] R.J.C. Vaessen, M.M. Seckler, G.J. Witkamp, "Heat transfer in scraped eutectic crystallizers", *International Journal of Heat and Mass Transfer*, Vol. 47, 2004, pp. 717–728.
- [8] Frank G.F. Qin, Xiao Dong Chen\*, Mohammed M. Farid, "Growth kinetics of ice films spreading on a subcooled solid surface", *Separation and Purification Technology*, Vol.39, 2004, pp.109–121.
- [9] J. Bellas, I. Chaer, S.A. Tassou, "Heat transfer and pressure drop of ice slurries in plate heat exchangers", *Applied Thermal Engineering*, Vol. 22, 2002, pp.721–732.
- [10] E. Nørgaard., T.A. Sørensen, T.M. Hansena, M. Kauffeld, "Performance of components of ice slurry systems: pumps, plate heat exchangers, and fittings", *International Journal of Refrigeration*, Vol. 28, 2005, pp. 83–91.
- [11] Mohamed Ben Lakhdar , Rosalia Cerecero , Graciela Alvarez , Jacques Guilpart , Denis Flick , Andr Lallemand, "Heat transfer with freezing in a scraped surface heat exchanger", *Applied Thermal Engineering*, Vol. 25, 2005, pp. 45–60.
- [12] David MacPhee, Ibrahim Dincer, "Performance assessment of some ice TES systems", *International Journal of Thermal Sciences*, Vol. xxx, 2009, pp 1–12.
- [13] Jorge L. Alvarado a, Charles Marsh , Chang Sohn , Gary Phetteplace , Ty Newell, "Thermal performance of microencapsulated phase change material slurry in turbulent flow under constant heat flux", *International Journal of Heat and Mass Transfer*, Vol. 50, 2007, pp.1938–1952.
- [14] C B. Frei, H. Huber, "Characteristics of different pump types operating with ice slurry", *International Journal of Refrigeration*, Vol. 28, 2005, pp.92–97.
- [15] Frank Qin , Xiao Dong Chen, Shashini Ramachandra , Kevin Free, "Heat transfer and power consumption in a scraped-surface heat exchanger while freezing aqueous solutions", *Separation and Purification Technology*, Vol. 48, 2006, pp.150–158.
- [16] Takaaki Inada, Poly Rani Modak, "Growth control of ice crystals by poly(vinyl alcohol) and antifreeze protein in ice slurries", *Chemical Engineering Science*, Vol. 61, 2006, pp.3149–3158.
- [17] Vincent Ayl, Olivier Lottin , Elena Popa , Hassan Peerhossaini, "Using undercooling to measure the freezing points of aqueous solutions", *International Journal of Thermal Sciences*, Vol.44, 2005, pp.11–20.
- [18] Hiroyuki Kumano, Tatsunori Asaoka, Akio Saito, Seiji Okawa, "Study on latent heat of fusion of ice in aqueous solutions", *International Journal of Refrigeration*, Vol.30, 2007, pp. 267-273.

- 
- 
- [19] Koji Matsumotoa,, Ken Oikawab, Masashi Okadac, Yoshikazu Teraokad, Tetsuo Kawagoe, “Study on high performance ice slurry formed by cooling emulsion in ice storage (discussion on adaptability of emulsion to thermal storage material)”, *International Journal of Refrigeration*, Vol.29, 2006, pp.1010-1019.
- [20] Jacques Guilpart, Evangelos Stamatou, Anthony Delahaye, Laurence Fournaison, “Comparison of the performance of different ice slurry types depending on the application temperature”, *International Journal of Refrigeration*, Vol. 29, 2006, pp. 781–788.
- [21] A. Melinder, E. Granryd, “Using property values of aqueous solutions and ice to estimate ice concentrations and enthalpies of ice slurries”, *International Journal of Refrigeration*, Vol. 28, 2005, pp.13–19.
- [22] Rajinder Singh and S. S. Kachhwaha, “Development of Scraped Surface Ice Slurry Generator”, *ASHRAE India Chapter Newsletter*, Vol. 12, issue 2, 2010.
- [23] Rajinder Singh and S. S. Kachhwaha, “Effect of antifreeze mass fraction on ice slurry generation in a scraped surface ice slurry generator”, *ASHRAE India Chapter Newsletter*, Vol. 12, issue 4, 2011.
- [24] O.Lottin, C. Epiard, “Dependence of the thermodynamic properties of ice slurries on the characteristics of marketed antifreezes”, *International Journal of Refrigeration*, Vol. 24, 2001, pp. 455–467.

---

---

# Comparison of Fourth Generation Refrigerants HFO 1234yf and 1234ze by Second Law Efficiency and Exergy Destruction Analysis for Automobile Sector

**Salma Khatoon<sup>1</sup>**

<sup>1</sup>Mechanical Engineering Dept., Jamia Millia Islamia , New Delhi, India

Email: salmakhatoon09@gmail.com

## **ABSTRACT**

The article presents the analysis of exergy for Vapour Compression Refrigeration System (VCRS) influenced by evaporator temperature. The analysis of the process and cycle is based on exergy destruction due to irreversibilities. The present work analyzed the behavior of four refrigerants of Vapour Compression Refrigeration System (VCRS) with variation in evaporator temperature. The analysis is influenced by the varied evaporator temperature and found that the capillary has unusual decreasing exergy destruction compared to the other devices. The result shows that as we decrease the temperature difference between the condenser and evaporator or for the fixed condenser temperature and increase in evaporator temperature, there is a gradual decrease in exergy destruction or improve in second law efficiency. The performances of these refrigerants are almost same with a little variation of R-12 and R-134a with R-1234ze and R1234yf. From our analysis, the performance of R-12 and R-134a are better than R-1234ze and R1234yf but refrigerant R-12 and R-134a are highly toxic and have high GWP (Global Warming Potential).

*Keywords—Exergy destruction , Second law efficiency, Automobile refrigeration system,*

## **1.0 INTRODUCTION**

The focus in reducing the global warming of our planet has led to consider the synthetic refrigerants with more uncertainty. Whilst in recent decades there has been considerable interest in rediscovering the use of natural fluids, in most real applications still dominate the synthetic fluids such as the hydro - fluoro-carbons (HFCs). These fluids, greeted with a considerable enthusiasm at the end of the last century for their zero ODP (Ozone Depletion Potential), now are considered particularly damaging to the environment because of their GWP (Global Warming Potential), which can be more than 1000 times that of carbon dioxide. In recent years, there have been some legislative procedures restricting the use of HFCs. In Europe, the phase-out of HFCs has already been scheduled and initiated on 1st of January, 2015 [7], banning the use of fluids with a GWP greater than 150 for the household refrigerators. Similar measures have been adopted in Japan while they are being studied in Canada, the United States and Mexico, where it is expected the beginning of the phase-out of HFCs as of January 1 of 2019 [8]. Therefore, an impending world needing to replace these refrigerants with others having low GWP

---

---

In some field, such as domestic refrigeration, it has already been proposed to replace HFC134a, reference fluid used from the 90s [9], with isobutane (R600a). However, although this solution has already been accepted by the European market, it involves some technical difficulties related to the high flammability of R600a. While the reduced amount of charge present in a domestic refrigerator for the European market is not of particular concern, the manufacturers of the household refrigerator had to redesign some areas of their production plant.

(i.e. warehouse storage of refrigerant, and charging stations), causing massive investments for the companies involved. Of no lesser importance is the adoption of specific components (i.e. the compressors) able to operate with HCs (Hydro-carbons). Also, as evidenced by Bansal et al. [10] the use of R600a may have high barriers to the American market (US market) because of more stringent standards for fire prevention (UL Standard 250), as well as other markets might be reluctant to such a solution. An alternative solution has been put forward with the introduction into the market of the fourth generation refrigerants: the hydro-fluoro-olefins (HFO) characterised by GWP values close to 1, such as HFO1234ze and HFO1234yf. The HFC/HFO mixtures have also been investigated and proposed as a possibility to perform a drop-in replacement HFC134a [11–14].

DuPont and Honeywell proposed the HFO-1234yf as the substitute for HFC-134a in MAC. And thermodynamic properties of HFO-1234yf were estimated by Thomas [5] using M-H EOS and the modeling results of the comparison between HFO-1234yf and HFC-134a showed that it behaved very similarly as HFC-134a did in refrigeration system. Its compatibility with motor, sealing materials and POE lubricants, the toxicity and the flammability properties was also investigated by Thomas. Park [6] studied the nucleate boiling heat transfer coefficients of HFC-134a and HFO-1234yf on a flat plain and low fin surfaces for the design and manufacture of high efficiency evaporators for HFO-1234yf. Four blends, AC-1, DP-1, JDH and fluid H possessing low GWP and using HFO-1234yf as ingredient [7], used to be considered as the substitutes for HFC-134a, but further consideration was ended because of their toxicity.

An interesting low GWP substitute for HFC134a is HFC152a, the unique HFC refrigerant with a GWP lower than 150 showing working pressures suitable for use in household appliances. Bolaji (2010) experimentally investigated the substitution of HFC134a with HFC152a and HFC32 in domestic refrigerators. The performance of HFC152a was constantly better than those of HFC134a and HFC32 both under cooling capacity and COP point of view. The HydroFluoroOlefin (HFOs) refrigerants, especially HFO1234yf and HFO1234ze(E), are other suitable candidates for HFC134a replacement in domestic and small refrigerators. Yana Motta et al. (2010) found that both HFO1234yf and

---

---

HFO1234ze(E) were suitable for drop-in replacement of HFC134a in small refrigerators. Karber et al. (2012) experimentally investigated the performance of HFO1234yf and HFO1234ze(E) as drop-in replacements for HFC134a in domestic refrigerators. HFO1234yf exhibits COP and cooling capacity similar to HFC134a, whereas HFO1234ze(E), although it performs favourably in term of COP, has a cooling capacity significantly lower than HFC134a and therefore it is unsuitable for direct drop-in replacement of HFC134a. Leighton et al. (2012) developed a simulation model of a commercially available HFC134a household refrigerator to evaluate the drop-in performance of several low GWP alternative refrigerants. HFO1234yf seems to be the most promising direct drop-in replacement for HFC134a in domestic refrigeration. This paper presents the comparative performance analysis of the low GWP refrigerants HFO1234yf, HFO1234ze(E) and HC600a inside a commercial roll-bond evaporator for household refrigerators.

## **2.0.LITERATURE REVIEWS**

A literature review was conducted in the specific area of analysis related to VCRS using R 1234yf and R1234ze. The literature available can be broadly classified as:

- Performance parameter
- Efficiency
- Exergy analysis

### **2.1 Performance parameter:**

Mahajan and Borikar find out that the performance of HC-12a in the domestic refrigerator condenser temperature and evaporator temperature, COP, refrigerating effect, condenser duty, work of compression and heat rejection of water are better than those of R134a throughout all the operating conditions. Venkataiah and Rao thermodynamically analysed R22, R134a, R404A, R407C, R410A, R507A, R290 and R600a using COOLPACK software .It focuses on fixed condenser temperature but with variable evaporator temperatures. Tashtoush et.al experimented on the replacement of R12 in domestic refrigerators by new hydrocarbon/ hydrofluorocarbon refrigerant mixtures. The results show that butane / propane / R134a mixtures provide excellent performance parameters, such as coefficient of performance of refrigerator, compression power, volumetric efficiency, condenser duty, compressor discharge pressure and temperature, relative to a 210 g charge of R12. ShengJun et.al evaluated the non-azeotropic mixtures containing HFOs as potential refrigerants in refrigeration and high-temperature heat pump system and found that it has higher COP than that of HFC-134a and served as a good environment friendly refrigerant. Righetti. Et.al compared the performance analysis of low GWP



---

---

refrigerants HFO 1234yf, HFO1234ze and HC600a inside a roll-bond evaporator and found that HFO1234yf has similar performance to HFC134a at the same mass flow rate.

## **2.2 Efficiency:**

Yadav and Nagalakshimi explore performance and efficiency variations of a refrigeration system using R12 and R134a refrigerant. Raja et.al did an analysis of energy and exergy on a traditional Vapor Compression Refrigeration Cycle using R152a, R290, R600, R600a, R123 and R717. The result deduced that these alternative refrigerant R600, R600a, R717 and R152a had higher COP and exergetic efficiency than R134a for evaporative temperature which range from 248 K to 283 K and condensation temperature 318 K with superheating 10 K and subcooling 5 K. Tare. et.al did the comparative study of exergy loss of refrigerants during condensation process of vcr cycle and a relationship between exergy drop and COP is established to optimize second law analysis of the system for different refrigerants for constant pressure condensation process in a vapour compression refrigerant cycle.

## **2.3 Exergy analysis :**

Xu and Clodic introduced an exergy analysis method on Vapour Compression Refrigeration Cycle in order to compare the performance between 3 refrigerators using R12, R134a and R290 as the refrigerants. The refrigerator of R134a is almost efficient than for R12. But freezers for R134a and for R290 are less efficient than R12 freezer. Zakirov and Karimov evaluated the efficiency of evaporators with rolled-up pipes by the exergy analysis method. Reddy et.al did an exergy analysis of a Vapour Compression Refrigeration Cycle with selected refrigerants and found that R134a has the better performance in all respect, whereas R407C refrigerant has poor performance. Lee et.al presents numerical analysis of exergy for air-conditioning influenced by ambient temperature. The result shows that reducing exergy loss of the capillary influenced by the ambient temperature is the key for improving working efficiency of an air-conditioning system. Yataganbaba. et.al done the exergy analysis of R1234yf and R1234ze as R134a replacement in a two evaporator vapour compression system and found that the lowest total exergy destruction is obtained by using R134a as a refrigerant while obtaining the highest ones with R1234yf in the refrigeration system

After reviewing it was found that there is a gap in work carried out in the field of total exergy destruction and second law efficiency and so it is proposed in this paper.

## **3.0 METHODOLOGY**

In the present analysis analytical method is used for comparison among automobile sector refrigerants on VCR system to analyze exergy destruction and second law efficiency.

---

### 3.1 Cycle description:

The vapor compression refrigeration cycle is the majorly applied refrigeration cycle, which consists of a compressor, condenser, throttling device and an evaporator with controls and interconnections. Fig. 1 exhibits the schema of a basic VCRS, which is a general irreversible cycle model.

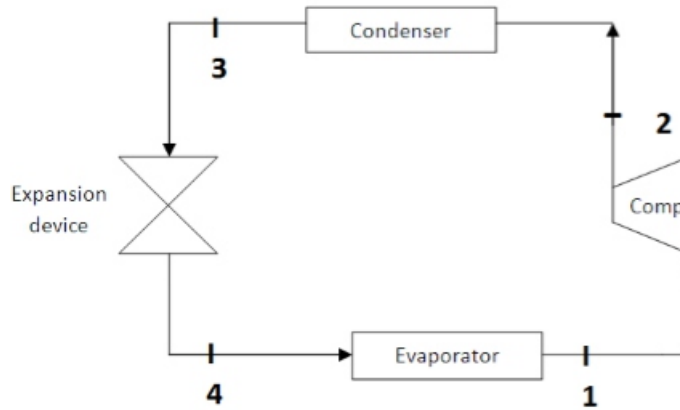


Fig. 1 Block Diagram of Basic Vapour Compression Refrigeration Cycle

The figure shows the different components of the vapour compression refrigeration cycle and the flow direction of the refrigerant cycle from the beginning with suction of the compressor, which is convenient to explain the procedure. In process, the refrigerant is first sucked and compressed by the compressor. At the exit of the compressor, the refrigerant is at extremely high pressure and superheated. The compressed refrigerant will flow into the condenser to be condensed and take place the heat exchange with the surroundings. The emitted heat of refrigerant during condensing in the condenser is transferred into the surroundings through the forced convection. The condensed refrigerant in the condenser outlet is directly led to the inlet of the throttling device and runs through the throttle device into the evaporator. The process of the evaporation for refrigerant in the evaporator will receive heat from the cooling space. After the evaporation of refrigerant in the evaporator, the refrigerant vapour is sucked again by the compressor and built the refrigeration cycle.

### 3.2 Refrigerant chosen and its properties:

For our analysis we have chosen 3 refrigerant, namely:

- R-1234yf
- R-1234ze
- R-134a
- R-12



---

---

### 3.2.1 R-1234yf

- It is compatible with motor and sealing materials.
- It has good miscibility in POE (Polyolester) lubricants.
- It has good thermal stability
- It has Zero ODP(Ozone depletion potential) and GWP (Global Warming Potential) 4-6.
- It has significant environmental benefits.

### 3.2.2 R-1234ze:

- Its flammability limits depends on the humidity of air. HFO1234ze which is non flammable in dry air but becomes flammable if humidity becomes larger than 10%.
- It is suitable for high temperature applications rather than in typical air conditioners.
- It has Zero ODP(Ozone depletion potential) and GWP (Global Warming Potential) 4-6.

### 3.2.4 R-12

- R-12 was the first fluorocarbon refrigerant developed and used commercially and is still a standard for comparing other refrigerant
- It has many properties especially suitable for use in refrigeration, such as good stability, little effect on elastomer and plastics, good solubility in lubricating oil and a reasonable compression ratio.
- Non-flammability, low toxicity, inertness and stability were also recognised as essential refrigerant property

### 3.2.5 R-134a:

- It produces high global warming potential.
- HFC – 134a is widely used as a replacement for CFC 12. It is used in various applications, such as domestic, commercial and industrial refrigeration and air-conditioning.
- The performance characteristics of HFC134a are similar to those of CFC 12.

## 3.3 Exergy Analysis.

The Exergy analysis bases on the basic vapour compression refrigeration system shown in Fig. 1. Numerical Modulation discussed the complete system and its four main devices separately. The applied vapour compression refrigeration system is defined to fit the following four assumptions:

### 3.3.1 Assumptions:

These are the assumptions for the vapour compression refrigeration system :

- Steady state, steady flow operation,
- Negligible pressure drops in the evaporator, condenser, and intersections,
- Adiabatic compression process,
- Isenthalpic expansion in expansion device,
- Negligible kinetic and potential energies.

Table 1 exhibits design parameters of the applied system. The efficiency of a vapour compression refrigeration cycle is indicated by the coefficient of performance (COP), which is defined by the amount of cooling energy per supplied work. The COP of a vapour refrigeration cycle is expressed as equation

$$\text{COP} = Q / W$$

Where Q is Cooling Energy and W is work input.

**Table 1 Design parameters of the applied vapour compression refrigeration system**

Parameter	Value
Refrigeration capacity	3.51 kW
Condenser Temperature	313K
Evaporator Temperature Range	243K ~ 293K
Refrigerants	R-12, R-1234yf, R-1234ze, R-134a
Ambient Temperature	298K
Isothermal efficiency	85%
Mechanical efficiency	84%
Electrical efficiency	90%

Referring to the main cycle loop in Fig. 1 from the first law of thermodynamics and a general relation for a cyclic process can be written as equations.

#### 4.0 EXERGY ANALYSIS :

Applying exergy balance equation

$$\dot{e}_1 + \dot{w}_c = \dot{e}_2 + \dot{I}_{12}$$

$$\dot{I}_{12} = (\dot{e}_1 - \dot{e}_2) + \dot{w}_c$$

$$\dot{I}_{12} = \dot{m}\{(h_1 - h_2) + T_o(S_2 - S_1)\} + \dot{w}_c$$

Since process is isentropic i.e.

$$S_1 = S_2$$

$$\dot{I}_{12} = \dot{m}(h_1 - h_2) + \dot{w}_c$$

---

Where,

$w_c$  is power input to the compressor (kW),

$m$  is mass flow rate of refrigerant (kg/s),

$h$  is enthalpy (kJ / kg ),

$T_o$  is the ambient temperature (K),

$I_{12}$  is exergy destruction in compressor (kW),

$S$  is the specific entropy (kJ/kg-K),

For actual cycle,

$$\eta_{iso} = 0.85$$

$$\eta_{mech} = 0.84$$

$$\eta_{elec} = 0.9$$

Considering mechanical and electrical exergy loss,

$$\begin{aligned} I_{(mech,elec)} &= w'_e - w_c \\ &= w'_e - \eta_{mech} \cdot \eta_{elec} \cdot w'_e \\ &= (1 - \eta_{mech} \cdot \eta_{elec})w'_e \end{aligned}$$

$$e_1 + w'_e = e'_2 + I'_{12}$$

$$I'_{12} = (e_1 - e'_2) + w'_e$$

$$I'_{12} = m\{(h_1 - h'_2) + T_o(S'_2 - S_1)\} + w'_e$$

Where,

$h'$  is actual enthalpy

$S'$  is actual entropy

$I'$  is actual exergy destruction

$w'_e$  is actual compression work or motor input

#### 4.2 Exergy of Condenser

$$e_2 = e_3 + \text{Exergy due to the heat loss to the surrounding} + I_{23}$$

Exergy due to the heat loss to the surrounding

$$= Q_c (1 - T_o/T)$$

Since the surrounding is assumed to be at dead state

Therefore,  $T = T_o$

Exergy due to heat loss to the surrounding = 0

$$I_{23} = e_2 - e_3$$

$$I_{23} = m\{(h_2 - h_3) + T_o(S_3 - S_2)\}$$

#### 4.3 Exergy of Expansion valve

$$e_3 = e_4 + I_{34}$$

$$I_{34} = m\{(h_3 - h_4) + T_o(S_4 - S_3)\}$$

Since it is as isenthalpic process

Therefore,  $h_3 = h_4$

$$I_{34} = m T_o(S_4 - S_3)$$

#### 4.4 Exergy of Evaporator

$$\dot{e}_4 + Q_e(1 - T_o/T_e) = \dot{e}_1 + I_{41}$$
$$I_{41} = (\dot{e}_4 - \dot{e}_1) + Q_e(1 - T_o/T_e)$$

Since,  $T_o > T_e$

$$Q_e(1 - T_o/T_e) = -ve$$

i.e. decrease in exergy of the system so we have to supply the external exergy in the form of compressor work.

Total exergy destruction ( $I_{totaldest}$ ) is given by,

$$I_{total\ dest} = I_c + I_{cond} + I_{expn} + I_{evap}$$

The second law efficiency of the system is the ratio of actual COP and ideal COP.

$$\eta_{II} = \frac{(COP)_{actual}}{(COP)_{ideal}}$$

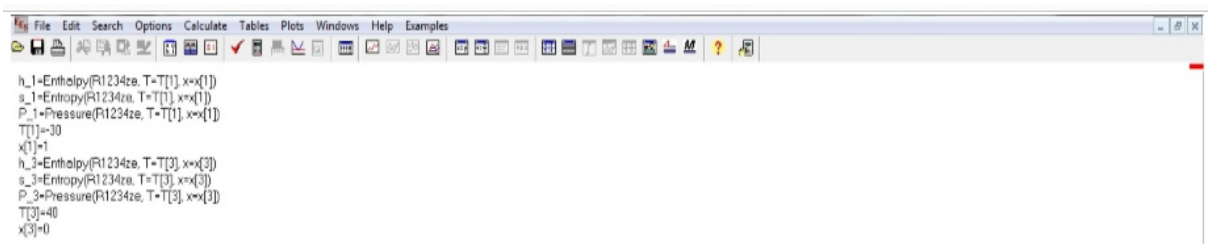
$$(COP)_{ideal} = T_c / (T_c - T_e)$$

$$(COP)_{actual} = \text{Refrigeration capacity} / w'_e$$

### 5.0 EES (ENGINEERING EQUATION SOLVER)

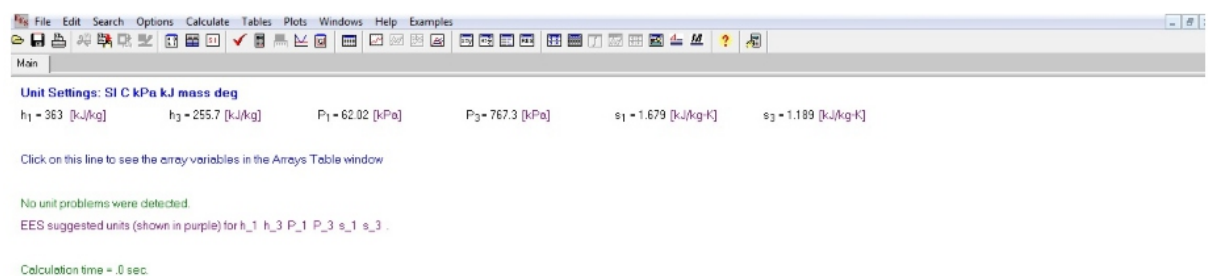
Engineering Equation Solver (EES) is a well known software used for solution of systems of simultaneous non-linear equations. EES performs the iterative solving, eliminating the tedious and time-consuming task of acquiring thermodynamic properties with its built-in functions. EES also includes parametric tables that allow the user to compare a number of variables at a time. Parametric tables can also be used to generate plots.

EES32 has been used to find enthalpy, entropy and pressure at different state points for R-1234ze and R-1234yf. An example for R-1234ze has been shown in Fig.2 and Fig.3.



```
h_1=Enthalpy(R1234ze, T=T[1], x=x[1])
s_1=Entropy(R1234ze, T=T[1], x=x[1])
P_1=Pressure(R1234ze, T=T[1], x=x[1])
T[1]=30
x[1]=1
h_3=Enthalpy(R1234ze, T=T[3], x=x[3])
s_3=Entropy(R1234ze, T=T[3], x=x[3])
P_3=Pressure(R1234ze, T=T[3], x=x[3])
T[3]=40
x[3]=0
```

Fig.2. Equations for different properties for R-1234ze in EES32



Unit Settings: SI C kPa kJ mass deg

$h_1 = 363$ [kJ/kg]	$h_3 = 255.7$ [kJ/kg]	$P_1 = 62.02$ [kPa]	$P_3 = 767.3$ [kPa]	$s_1 = 1.679$ [kJ/kg-K]	$s_3 = 1.189$ [kJ/kg-K]
---------------------	-----------------------	---------------------	---------------------	-------------------------	-------------------------

Click on this line to see the array variables in the Arrays Table window

No unit problems were detected.

EES suggested units (shown in purple) for  $h_1$   $h_3$   $P_1$   $P_3$   $s_1$   $s_3$ .

Calculation time = 0 sec.

Fig.3. Results obtained for different properties for R-1234ze by EES32

---

## 5.0 RESULTS:

### 5.1 Variation of exergy destruction with Evaporator temperature

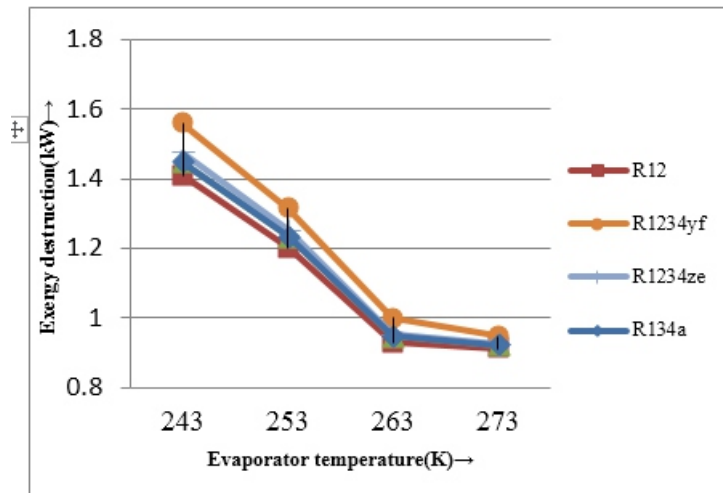


Fig. 4. Variation of exergy destruction with Evaporator temperature

### 5.2 Variation of second law efficiency with Evaporator temperature.

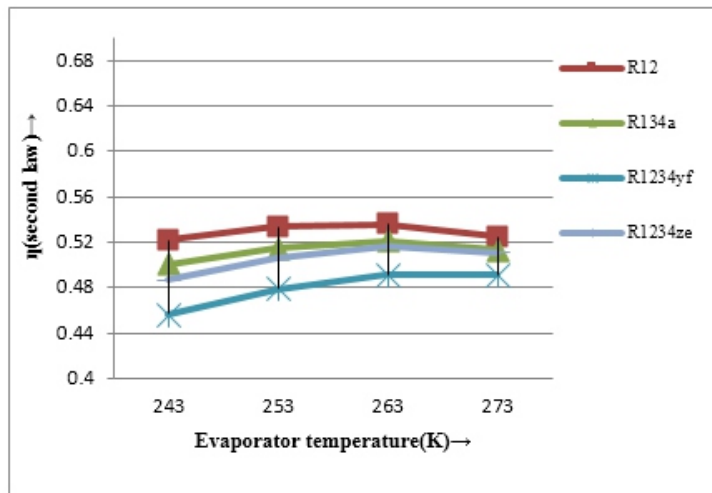


Fig.5.Variation of second law efficiency with Evaporator temperature.

## 6.0 CONCLUSION

As we decrease the temperature difference between the condenser and evaporator or for the fixed condenser temperature and increase in evaporator temperature, there is a gradual decrease in exergy destruction or improve in second law efficiency for different refrigerant (i.e. R-12, R-134a, R-1234ze and R-1234yf) as obvious from clausius statement. The performance of these refrigerant are almost same with a little variation of R-12 and R-134a with R-1234ze and R-1234yf. From our analysis, the

---

---

the performance of R-12 and R-134a are better than R-1234ze and R-1234yf but refrigerant R-12 and R-22 are highly toxic and have high GWP (Global Warming potential).

## REFERENCES

- [1] Zaghoudi M.C., S.Maalej, Y.Saad and M.Bouchaala, *A Comparative study on the Performance and Environmental Characteristics of Alternatives to R22 in Residential Air Conditioners for Tunisian Market*, *Journal of Environmental science and Engineering*, Volume 4, No.12 (2010).
- [2] Devotta S.,Waghmare A. V.,Sawant N.N and Domkundwar B.M. *Alternatives to HCFC-22 for air conditioners Applied thermal Engineering*, volume 21 (2001) pp703-715.
- [3] Domanski P.A and, Didion D.A., *Thermodynamic evaluation of R-22 alternative Refrigerants and Refrigerant mixtures*, *Ashrae Transactions* 99(1993) pp636-648 part 2.
- [4] Murat Hozod (2005). "Performance Comparison of Single-Stage and Cascade Refrigeration Systems Using R134a as the Working Fluid," *Turkish J. Eng. Env. Sci* Vol 29, 285-269.
- [5] Rotchana Prapainnop, K O Suen (2012). "Effects of refrigerant properties on refrigerant performance comparison: A review," *International Journal of Engineering and Research and Applications* Vol. 2, pp. 486-493.
- [6] Guo-liang Ding (2007). "Recent developments in simulation techniques for vapour-compression.
- [7] Miguel Padilla, Remi Revellin, Jocelyn Bonjour (2010). "Exergy analysis of R413A as replacement of R12 in a domestic refrigeration system," *Energy Conversion and Management* Vol. 51, 2195-2201.
- [8] M. Y. Taib, A. A. Aziz, A. B. S. Alias (2010). "Performance Analysis of a Domestic Refrigerator," *National Conference in Mechanical Engineering Research and Postgraduate Students*.
- [9] Abhishek Tiwari, R. C. Gupta (2011). "Experimental Study of R-404A and R-134A in Domestic Refrigerator," *International Journal of Engineering Science and Technology* Vol. 3, 6390-6393.
- [10] J. K. Dabas, A. K. Dodeja, Sudhir Kumar, K. S. Kasana (2011). "Impact of Refrigerant Charge over the Performance Characteristics of a Simple Vapour Compression Refrigeration System," *International Journal of Advances in Engineering and Technology* Vol. 1, pp. 267-277.
- [11] N. Subramani, M. J. Prakash (2011). "Experimental studies on a vapour compression system using nano refrigerants," *International Journal of Engineering Science and Technology* Vol. 3, pp. 95-102.
- [12] S. J. Sekhar, D. M. Lal (2005). "HFC 134a/HC600a/HC290 mixture a retrofit for CFC12 systems," *International Journal of Refrigeration* Vol. 28, 735-743.
- [13] I. M. Mahbulul, S. A. Fadhilah, R. Saidur, K. Y. Leong, M. A. Amalina (2013). "Thermo physical properties and heat transfer, Performance of Al2O3 /R-134a nanorefrigerants," *International Journal of Heat and Mass Transfer* Vol. 57, 100-108.
- [14] Min Zhang, Ruixiang Wang, Jiangfeng Lou (2011). "Actuality and application foreground of nanofluids in refrigeration," *Materials Science Forum* Vol. 694, 261-265.
- [15] I. M. Mahbulul, R. Saidur, M.A. Amalina (2011). "Pressure Drop Characteristics of TiO2 -R123 Nano refrigerant in a Circular Tube," *Engineering e-Transaction* Vol. 6, pp. 124-130.
- [16] Ching-Song Jwo, Chen-Ching Ting, Wei-Ru Wang (2009). "Efficiency analysis of home refrigerators by replacing hydrocarbon refrigerants," *Measurement* Vol. 42, 697-701.
- [17] B. O. Bolaji, M.A. Akintunde, T. O. Falade (2011). "Comparative Analysis of Performance of Three Ozone-Friends HFC Refrigerants in a Vapour Compression Refrigeration," *Journal of Sustainable and Environment* Vol. 2, 61-64.
- [18] Z..ShengJun\*, W. HuaiXin, G. Tao (2010), "Evaluation of non-azeotropic mixtures containing HFOs as potential refrigerants in refrigeration and high-temperature heat pump systems" Vol-53(7),1855-1861.
- [19] Y.Lee, D.Kang, D. Jung (2013), "Performance of virtually non-flammable azeotropic HFO1234yf/HFC134a mixture for HFC134a applications" *International journal of refrigeration*, vol- 36,1203-1207.
- [20] G.A.Longo, S.Mancin, G. Righetti, C. Zilio(2016). "HFO1234ze(E) vaporisation inside a Brazed Plate Heat Exchanger (BPHE): Comparison with HFC134a and HFO1234yf. *International journal of refrigeration*, vol- 67,125-133.
- [21] C. Aprea, A. Greco , A. Maiorino(2016), "An experimental investigation on the substitution of HFC134a with HFO1234YF in a domestic refrigerator".*Applied thermal engineering* vol-106,959-967.
- [22] G. Righetti, C. Zilio, G. A. Longo (2015), "Comparative performance analysis of the low GWP refrigerants HFO1234yf, HFO1234ze(E) and HC600a inside a roll-bond evaporator".*International journal of refrigeration*,vol-54, 1-9.

---

---

# Choice Of Static Var Compensator (SVC), Modeling And Determination Of Its Power Factor Correction (PFC) Capability In A.C. Transmission Line

**Ibekwe B.E. Ph.D<sup>1</sup>, TChiwetalu U. J.<sup>2</sup> Eje, B.E<sup>3</sup>**

<sup>1</sup>Department of Electrical and Electronic Engineering, Faculty of Engineering Enugu State University of Science and Technology (ESUT), Enugu

<sup>2</sup>Department of Agricultural and Bio-resources Engineering, Faculty of Engineering Enugu State University of Science and Technology (ESUT)

<sup>3</sup>Department of Agriculture and Bio-resource Engineering, Enugu State University of Science and Technology

## **ABSTRACT**

The Power Factor Correction (PFC) capability of Static Var Compensator (SVC) in a.c. transmission line is presented. SVC P.F.C capability is very important because it can help to adjust the line reactive power to control the system voltage. This is implemented by using a circuit configuration of self-commutated Pulse Width Modulation (PWM) converter system consisting of Thyristor Controlled Reactor (TCR) and Fixed Capacitors (FC). The end result is that the line current tracked the voltage, thus improving the system PF significantly to about 98%.

*Keywords—*a.c. transmission line, SVC, PFC, PWM converters, Flexible AC Transmission System (FACTS).

## **INTRODUCTION**

Of all the FACTS controllers researched, which included the first and the second generation of these devices, the SVC was chosen based on the following simple reasons: [3]

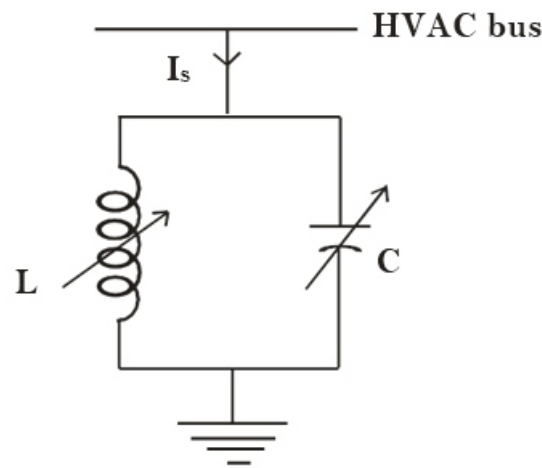
- It is capable of providing continuous and rapid control of reactive power and voltages.
- It can enhance several other aspects of transmission line performance such as:
  - (i) Control of temporary (power frequency) over voltages
  - (ii) Prevention of voltage collapse
  - (iii) Enhancement of transient stability
  - (iv) Enhancement of damping of system oscillation

At the sub-transmission and distribution system levels, SVCs are used for balancing the unbalanced three phase system supplying unbalanced loads. They are also used to minimize fluctuations in supply

voltage caused by repetitive-impact loads e.g. the dragline loads of mining plants, rolling mills and arc-furnaces [6].

### Development of the SVS Model

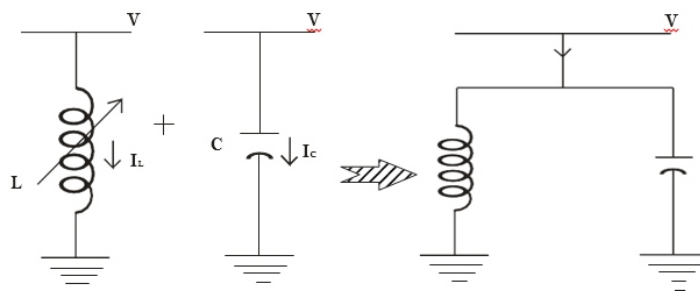
From power system operation viewpoint, the static var system (SVS) is equivalent to a shunt capacitor and a shunt inductor both of which can be adjusted to control voltage and reactive power at its terminals or nearby bus in a prescribed manner. Figure 2.1 is an idealized static var system model [1].



**Fig. 2.1: Idealized static var system model**

An ideal SVS should hold constant voltage, possess unlimited var generation/absorption capability with no active or reactive power losses [6].

However, the realistic or practical SVS is composed of a controllable reactor and a fixed capacitor. The resulting characteristics are essentially applied to a wide range of practical SVS configurations. Figure 2.2 illustrates the derivation of the characteristics of an SVS, made up of a controllable reactor and a fixed capacitor (FC). The component characteristic is derived by adding the individual characteristics of the components as shown [1].





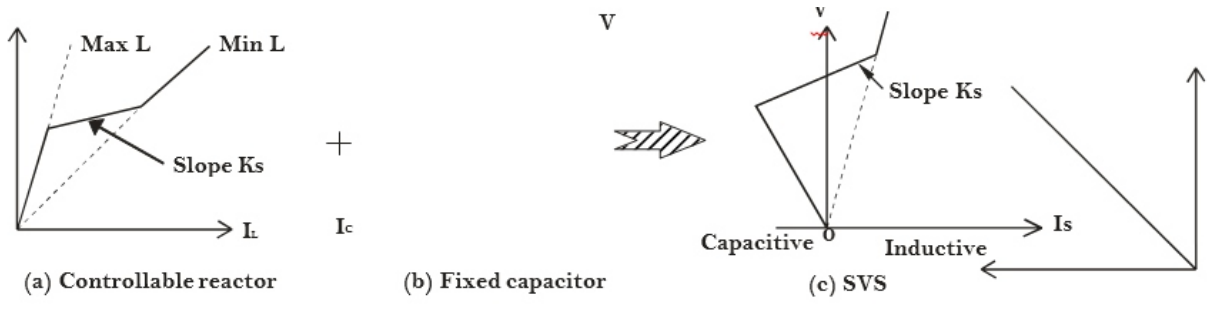


Figure 2.2 composite characteristics of an SVS

The basic elements of a Thyristor Controlled Reactor (TCR) are a reactor in series with a bidirectional thyristors switch (Fig. 2.3). The thyristors conduct on alternate half-cycles of supply frequency depending on the firing angle  $\alpha$  measured from a zero crossing of voltage.

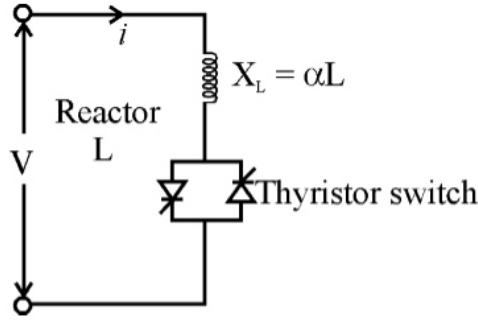


Figure 2.3: Basic Elements of TCR

Let  $\sigma$  be the conduction angle, related to  $\alpha$  by  
 $\sigma = 2(\pi - \alpha)$  ..... 2.1 [1].  
 Fourier analysis of the current waveform gives the fundamental components.

$$I_1 = \frac{V \sigma \sin \sigma}{X_L \pi} \dots \dots \dots 2.2 [1].$$

In effect, the TCR is a controllable susceptance. The effective susceptance as a function of the firing angle  $\alpha$  is given by:

$$B \propto \frac{I_1}{V} = \frac{\sigma \sin \sigma}{\pi \times L} \dots \dots \dots 2.3 [1].$$

Substituting equation 2.1 into 2.3 gives

$$B \propto \frac{2 \alpha - \sigma + \sin 2\alpha}{\pi \times L} \dots \dots \dots 2.4 [3].$$

Where  $\Sigma$  is the conduction angles

$X_L$  is the reactance of the reactor at a fundamental frequency.  
 From equation 2.3 and 2.4, the system voltage is given by:

$$V = \frac{L\pi X_L}{2\alpha - \sigma + \sin 2\alpha} \dots\dots\dots 2.5 [3].$$

**SVC Power Factor Correction (PFC) Capability in Power System**

Power factor correction (PFC) can be defined as a way of counteracting the undesirable effects of electric load that create power factor less than unity [3]. To determine the SVC PFC capability in a system is very important because it helps to adjust the reactive power to control the system voltage. To implement this, a circuit configuration with a resistive load consisting of TCR +FC, obtained from self-commutated PWM converter system was used.

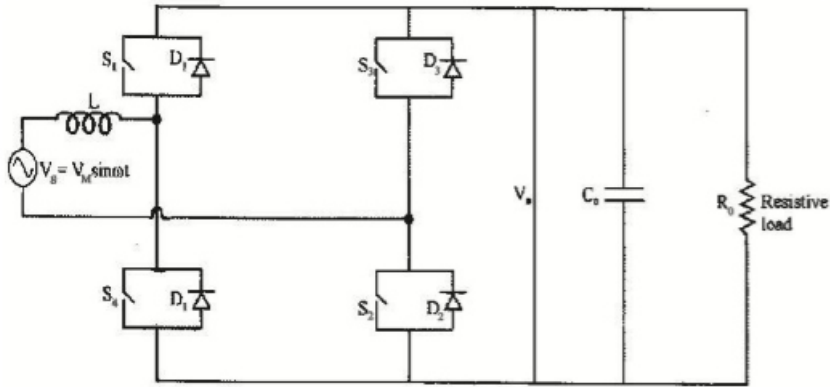


Figure 3.1: Circuit 1 with a resistive load

**Analysis of the Circuit**

(a)  $S_1, S_2$  closed (current decreasing):

Current loop:  $V_s \rightarrow L \rightarrow D_1 \rightarrow V_o \rightarrow D_2 \rightarrow V_s$

Equation:

$$\begin{aligned}
 V_s - L \frac{di_s}{dt} - V_o &= 0 \\
 \frac{di_s}{dt} &= (1/L) [V_s - V_o] \\
 &= [V_m \sin \omega t - V_o] / L
 \end{aligned}
 \tag{3.1}$$

Again,

$$i_c = C \frac{dV_o}{dt}$$

$$i_R = \frac{V_0}{R}$$

$$\frac{1}{S} = \frac{1}{C} + \frac{1}{R} = C \frac{dV_0}{dt} + \frac{V_0}{R} = 0$$

$$i_S - C \frac{dV_0}{dt} - \frac{V_0}{R} = 0$$

$$\frac{V_0}{dt} \left( \frac{1}{C} \right) \left[ \frac{1}{R} \right] = \frac{V_0}{R}$$

3.2

**(b)  $S_3, S_4$  closed (current increasing):**

Current loop:  $V_s \rightarrow L \rightarrow S_4 \rightarrow V_0 \rightarrow S_3 \rightarrow V_s$

Equation:

$$V_s - \frac{L di_S}{dt} + V_0 = 0$$

$\underbrace{\frac{1}{L} [V_s + V_0]}_{\text{current increasing}}$

$$\frac{di_S}{dt} = (1/L) [V_m \sin \omega t + V_0]$$

3.3

Again,

$$i_C = C \frac{dV_0}{dt}$$

$$i_R = \frac{V_0}{R}$$

$$i_S - i_C - i_R$$

$$\therefore i_S = -C \frac{dV_0}{dt} - \frac{V_0}{R}$$

$$i_S + C \frac{dV_0}{dt} + \frac{V_0}{R} = 0$$

$$C \frac{dV_0}{dt} = -i_S \frac{R}{R}$$

$$\therefore \frac{dV_0}{dt} = \frac{-1}{C} [I_S + V_0/R]$$

3.4

---

---

## Simulation Results

The circuit equations were loaded with the parameters defined below

$V_s = 220\sqrt{2}$  ,  $\omega t = 2\pi ft$ , switching period 4kHz. Assume ac and dc input power filters as  $L = 5\text{mH}$ ,  $C = 0.6\text{F}$ , and load resistance of  $R = 20\Omega$ . And the four equations were solved in MATLAB using Runge-Kuta; thus the plot of the output voltage and current waveforms are shown in figure 3.2.:

## 4. CONCLUSION

The computer simulated curves for Figure 3.2 showed that current had tracked the voltage thus, improved the power factor significantly to about 98%. Note that a high load power factor brings about an overall system balance in addition to the following:

- (i) Improvement of voltage regulation
- (ii) Enhancement of transmission system efficiency
- (iii) Elimination of current harmonic components in a system. Hence, power factor correction is an important tool to control the reactive power and improve the system voltage.

## REFERENCES

Edwards, C. et al (1986); "Advanced Static Var Generator Employing G.T.O. Thyristors" *IEEE Trans. on Power Delivery*, Vol. 3, No. 4, pp. 1622 – 1627.

Hadi Saadet (2004); *Power System Analysis, Second Edition. McGraw-Hill Publication.*

Ibekwe, B.E. et al (2014); *Girding Principles in selecting a.c to d.c Converters for Power Factor Correction in a.c Transmission System, IJERA Publication.*

Prabha Kundur (2010); *Power System Stability and Control, Tata, McGraw-Hill Edition.*

Walker, L. (1986); "Force-Commutated Reactive Power Compensation", *IEEE Trans. Industrial Application*, Vol. IA – 22, No. 6, Pp 1091 – 1104.

---

---

## Self Heating Effects In Soi Technology

**<sup>1</sup>Prem Prakash Satpathy, <sup>2</sup>Dr. Vijay Nath, <sup>3</sup>Abhinandan Jain**

<sup>1</sup> Lecturer, Dept. of ECE, Cambridge Institute of Technology, Ranchi

<sup>2</sup> HOD, Dept. of VLSI, BIT Mesra, Ranchi

<sup>3</sup>HOD, Dept. of ECE, Pratap University, Jaipur

### **ABSTRACT**

For more than three decades, it has been searching for a way to enhance existing silicon technology to speed up the computer performance. The Silicon on Insulator (SOI) technology results in faster computer chips with low frequency noise that also require less power a key requirement for extending the battery life of small, hand-held devices that will be pervasive in the future. SOI is a major breakthrough because it advances chip manufacturing one to two years ahead of conventional bulk silicon. It provides a step-by- step look at the developments leading up to the development of SOI technology. Increased demand for High Performance, Low Power and Low Area among microelectronic devices is continuously pushing the fabrication process to go beyond ultra deep sub-micron (UDSM) technologies such as 45nm, 32nm and so on. Currently, chips are being designed in 55nm, 45nm and 32nm process nodes. The performance and power goals for certain applications in these advanced nodes couldn't be achieved with conventional silicon bulk Complementary Metal oxide semiconductor (CMOS) process leading to an alternative, Silicon on Insulator SOI process. Silicon on Insulator fabrication process helps in achieving greater performance and offers less power consumption compared to the Bulk Process.

**Keywords—***Self-heating, impact ionization, kink effect, thermal conductivity, TCAD*

### **SELF HEATING EFFECTS IN SOI TECHNOLOGY:**

The presence of buried oxide could make the temperature of the channel rise more than in a classical transistor on Bulk, especially in the case of continuous current flow e.g. in analog biasing circuits is defined as self heating in SOI. Due to thermal isolation of substrate by the buried insulator in an SOI transistor, removal of excess heat generated by the Joule effect within the device is less efficient than in bulk, which leads to substantial elevation of device temperature. The excess heat mainly diffuses vertically through the buried oxide and laterally through the silicon island into the contacts and metallization. Due to the relatively low thermal conductivity of the buried oxide, the device heats up to 50°C to 150°C. This increase in device temperature leads to a reduction in mobility and current drive, thus degrading the device performance over a period of time.

Impact Ionization: If kink effect is attributed entirely to impact ionization effects then  $I_{ds} = I_{dso} + I_{kink}$  with  $I_{kink} = M I_{dso}$  where  $I_{dso}$  is the current that would be obtained if impact ionization effects were absent. When impact ionization is present, it provides a source of current and the electron current equation has the modified form impact ionization source is usually modeled by  $G I - I = -\alpha n J n$  with  $\alpha n = A n \exp(-\beta n / F)$  with  $n \alpha$  strongly dependent on the electric field strength  $F$ .

### Floating Body and Parasitic Bipolar Effects

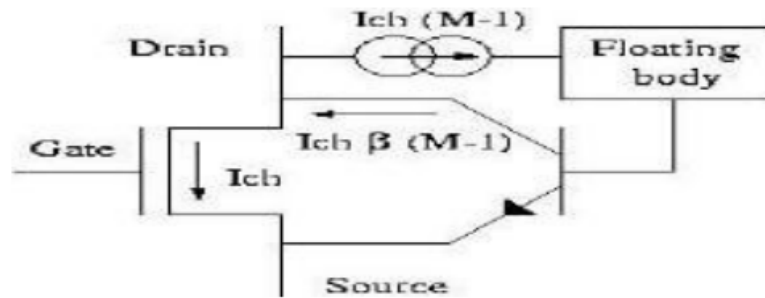
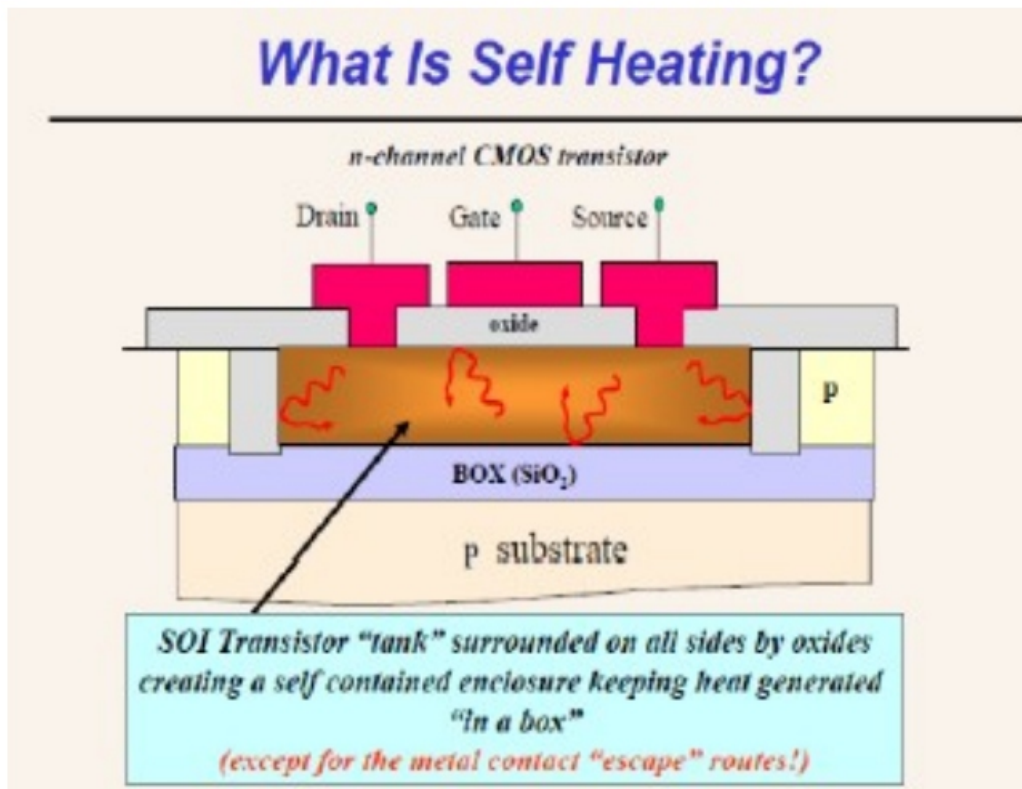


Figure 1.1 Parasitic bipolar transistor of the SOI MOSFET

The presence of a floating volume of silicon beneath the gate is at the origin of several effects unique to SOI, generically referred to as floating body effects. There exists a parasitic bipolar transistor in the MOS structure. If we consider an n-channel device, the N+ source, the P-type body and the N+ drain indeed form the emitter, the base, and the collector of an NPN bipolar transistor, respectively. In a bulk device, the base of the bipolar transistor is usually grounded by means of a substrate contact. But, due to the floating body in an SOI transistor, the base of the bipolar transistors is electrically floating. This parasitic bipolar transistor in figure 1.1 is origin of several undesirable effects in SOI devices.

### SELF HEATING EFFECT

These effects arise in SOI devices because the device is thermally insulated from the substrate by the buried oxide BOX. Consequently, removal of excess heat generated within the device by device switching is not removed as efficiently in SOI devices as it is in bulk devices. This leads to a substantial elevation of temperature within the SOI device 50°- 150°C as shown in figure 1.2. This self-heating effect only appears when power is being dissipated within the device that is when the transistor is on, conducting current through its channel. This only occurs in CMOS circuits when a logic stage is switching state, not when it is in a stand-by state e.g., holding logic high or low state.



**Figure 1.2 Self heating effects in SOI transistor**

These effects certainly will not prevent the widespread adoption of SOI for CMOS ICs, but they must be taken into account by thoughtful device and circuit design approaches that specifically address the peculiarities of the SOI CMOS transistor vs. the bulk or epitaxial wafer CMOS transistor. Obviously, the process simulation, device simulation, circuit simulation, and layout Technology Computer Aided design (TCAD) tools employed by designers must accurately model the peculiarities and advantages of SOI CMOS to achieve optimal device design, circuit design, layout and processing approaches for CMOS ICs fabricated with SOI wafers. CMOS transistors designed for use with SOI wafers are classified by the thickness of the device-quality single-crystal silicon layer at the surface above the BOX relative to the depths of the source-drain junction and channel depletion layers in the device with the operating voltages applied. An SOI CMOS transistor is classified as “partially depleted” (PD) if the silicon surface layer is thicker than the depth of the depletion region in the transistor's channel. The SOI CMOS transistor is classified as “fully depleted” (FD) if the silicon surface layer is equal to the depth of the depletion region in the transistor's channel. The transistor will be partially depleted or fully depleted depending on the silicon layer thickness above the BOX and the doping concentration in the channel. To form a fully depleted SOI transistor, the channel doping concentration must be low enough the gate depletion region extends throughout the entire thickness of the silicon layer. When the silicon surface layer is thicker than about 200nm, the transistor will typically be partially depleted, unless the channel

---

---

doping concentration is reduced to such low values that the threshold voltage is too low for practical CMOS applications less than 100mV. If the silicon layer thickness is reduced to about 100nm, the transistor will be fully depleted, even when the channel doping concentration is increased to produce threshold voltages of 300-400mV. If the silicon layer thickness is reduced further 70nm, the transistor will remain fully depleted even if the channel doping concentration is increased to produce even higher threshold voltages 700mV.

There are significant differences in partially depleted and fully depleted SOI CMOS transistors. For example, the threshold voltage of the fully depleted device is very sensitive to the silicon surface film thickness. This results in an additional source of manufacturing variance in the fabrication of FD SOI CMOS. Typically, this is in the order of 10mV in threshold voltage per nanometer of variation in the silicon film over the BOX. The fabrication of commercial CMOS on SOI typically employs partially depleted PD devices. However, careful device design and optimizing the channel implant process can reduce this sensitivity in FD devices. The variation of drain saturation current does not have the same sensitivity to film thickness as the threshold voltage in FD SOI CMOS. There are significant advantages for FD transistors over PD transistors, and the trend in SOI CMOS is toward the use of fully depleted devices. A fundamentally important point is that in FD SOI CMOS the sub threshold slope can be very low less than ~65 mV/decade i.e., a 65 mV increase in gate voltage will result in a tenfold increase in the sub threshold drain current. The differential equation describing heat transfer is:

$$\nabla^2 T = \frac{c\rho}{\lambda} \frac{\partial T}{\partial t}$$

- $\lambda$ : thermal conductivity, [W/m°C]
- $c$ : specific heat, [J/kg°C]
- $\rho$ : material density, [kg/m<sup>3</sup>]
- $T$ : temperature, [°C]
- $\lambda/c\rho$ : thermal diffusivity, [m<sup>2</sup>/s]

These effects arise in SOI devices because the device is thermally insulated from the substrate by the buried oxide (BOX). Consequently, removal of excess heat generated within the device by device switching is not removed as efficiently in SOI devices as it is in bulk devices. This leads to a substantial elevation of temperature within the SOI device 50°- 150°C.



---

---

The insulation layer of the SOI wafer creates a potential temperature delta between devices called local (self) heating. Self-heating is evident at the high power regions. It May not have huge impact on Digital circuits; however this effect must be considered for analog type of circuits. As CMOS technology scales down to deep sub-micron dimensions, power density increases accordingly, thus resulting in remarkable temperature increases in the active devices. This problem has become even more critical with the introduction of SOI technologies, where the low thermal conductivity of the insulation layer below the top silicon film inhibits an efficient heat flow through the substrate as in standard bulk CMOS technologies. Semiconductor components are really sensitive to temperature variations. The impact of raised operating temperatures in both analog and digital circuits increases self heating effect. Self heating in SOI can cause device and interconnect temperatures to raise more than 10°-12°C.

The self Heating effects can be summarized as follows:

- Degraded carrier mobility which leads to a reduced on-current of transistors and thus slower speed
- Higher interconnect metal resistivity which yields longer delays
- Increased failure rate
- Reduced reliability of electronic devices, with secondary effects such as interconnect electromigration

Self-heating phenomena are studied from room down to near liquid helium temperatures in fully depleted N channel thin film SIMOX MOS devices. A simple theoretical analysis of the self-heating effect is worked out. A method for the extraction of the thermal resistance and the device temperature rise directly from the static output characteristics is derived. Also direct self heating transient measurements are conducted.

SOI MOS devices are well known to suffer from self-heating phenomena arising from the low thermal conductivity of the buried oxide compared to Si substrate. At sufficiently high current levels, this result in the occurrence of negative output conductance in the saturation region. Self-heating effect is studied from room down to near liquid helium temperatures on fully depleted N channel thin film SIMOX MOS devices. Moreover, a simple self-heating model is proposed enabling the extraction of the thermal resistance and the average temperature rise of the device directly from the static output characteristics.

SOI devices suffer from the self-heating because of the existence of buried oxide BOX. Velocity overshoot should be considered to evaluate the self-heating effect in deep sub micrometer region. Drain current degradation due to the self heating effect in sub-0.1 μm SOI MOSFETs is investigated, focussing

---

---

on the comparison with bulk devices. It is revealed that the velocity overshoot can reduce the self-heating effect as well as the difference of the current degradation between SOI and bulk device.

In the bulk technologies, heat generated by charge transfer in the transistor is readily transferred out of the chip backside through silicon substrate. This transfer of heat is quick enough so that local device transconductance changes due to self-heating are negligible. For bulk devices with six or more layers of interconnect, the stacked inter-layer dielectrics ILDs present substantial thermal resistance. However, in the current generation of submicron technology bulk devices, these thermal issues are being addressed with the use of reduced dielectric constant dielectrics and higher conductivity metallization based on copper interconnect. In SOI technology, silicon dioxide comprises the BOX layer, so that the SOI transistor is encased in a perfect little insulated region of its own. As a result, the average junction temperature of SOI devices can be somewhat higher than for an identical bulk device, reducing the device transconductance. Since SOI transistors are thermally insulated from the substrate by the buried insulator, the removal of excess heat generated by the Joule Effect, within the device is less efficient than in the bulk devices. The excess heat has several conduction paths, diffusing vertically through the buried oxide and laterally through the silicon island into the contacts and the metallization.

Thus, SOI MOSFETs are susceptible to the local thermal heating generated in the channel due to less thermal conductivity of the buried oxide, which is approximately 100 times lower than thermal conductivity of silicon. The self-heating causes a reduction of the carrier mobility, shifts the threshold voltage, and results in a negative differential conductance at high gate and drain voltages. The negative resistance, which can be seen in the output characteristics of SOI Metal oxide semiconductor Field Effect Transistors (MOSFETs) is due to a mobility reduction effect caused by device self heating. This effect can compromise reliability of the part when the part is operating at low and ultra low temperatures due to thermo-mechanical stresses and possible formation of structural defects and microcracks.

## **CONCLUSION:**

In SOI devices, self-heating effect can be minimized by using a thin buried oxide film; thus, decreasing the bottom layer thermal resistance. Another advantage of this approach is the reduction of short channel effect for the back transistor. However, the back channel transistor threshold voltage is reduced if the doping level at the back channel interface is not increased. This, in combination with a floating body effect, can lead to a worst case behaviour. The self-heating effect is more pronounced in fully-depleted structures due to thinner silicon films, which means a thinner buried oxide will be required to minimize it. The limitation for thinning the buried oxide is imposed by the variations of the threshold

---

---

voltage with the backgate bias. Fully depleted devices exhibit a different electrical behaviour from the partially depleted devices. The threshold voltage varies with the backgate bias for enhancement mode and accumulation mode devices due to the coupling effect between the front and the back gates when the silicon film is fully depleted. As a result of this coupling effect, the threshold voltage of fully depleted devices becomes a function of the silicon and buried oxide thicknesses.

**REFERENCES:**

- [1] L. T. Su, et al., *IEEE trans. Electron Devices*, Vol. 41, no.1, p 69, Jan. 1994.
- [2] J. B. Roldan, et al., *IEEE Electron Device Lett.*, vol. 21, no.5, May 2000.
- [3] H. Kawashima and R. Dang, *IEICE Trans. Electron*. Vol. E82-C, p.894, 1999.
- [4] K. Matsuzawa, I. Kamohara and T. Wada, in *NASECODE VII*, P.173, 1991.
- [5] J. Jomaah, F. Balestra, and G. Ghibaudo, “ Self-heating effect in SOI MOSFETs operated at low temperature, ” in *SOI Conf. Dig.*, 1993, pp. 82-83.

# Instructions for Authors

## Essentials for Publishing in this Journal

- 1 Submitted articles should not have been previously published or be currently under consideration for publication elsewhere.
- 2 Conference papers may only be submitted if the paper has been completely re-written (taken to mean more than 50%) and the author has cleared any necessary permission with the copyright owner if it has been previously copyrighted.
- 3 All our articles are refereed through a double-blind process.
- 4 All authors must declare they have read and agreed to the content of the submitted article and must sign a declaration correspond to the originality of the article.

## Submission Process

All articles for this journal must be submitted using our online submissions system. <http://enrichedpub.com/> . Please use the Submit Your Article link in the Author Service area.

---

## Manuscript Guidelines

The instructions to authors about the article preparation for publication in the Manuscripts are submitted online, through the e-Ur (Electronic editing) system, developed by **Enriched Publications Pvt. Ltd.** The article should contain the abstract with keywords, introduction, body, conclusion, references and the summary in English language (without heading and subheading enumeration). The article length should not exceed 16 pages of A4 paper format.

### Title

The title should be informative. It is in both Journal's and author's best interest to use terms suitable. For indexing and word search. If there are no such terms in the title, the author is strongly advised to add a subtitle. The title should be given in English as well. The titles precede the abstract and the summary in an appropriate language.

### Letterhead Title

The letterhead title is given at a top of each page for easier identification of article copies in an Electronic form in particular. It contains the author's surname and first name initial .article title, journal title and collation (year, volume, and issue, first and last page). The journal and article titles can be given in a shortened form.

### Author's Name

Full name(s) of author(s) should be used. It is advisable to give the middle initial. Names are given in their original form.

### Contact Details

The postal address or the e-mail address of the author (usually of the first one if there are more Authors) is given in the footnote at the bottom of the first page.

### Type of Articles

Classification of articles is a duty of the editorial staff and is of special importance. Referees and the members of the editorial staff, or section editors, can propose a category, but the editor-in-chief has the sole responsibility for their classification. Journal articles are classified as follows:

#### Scientific articles:

1. Original scientific paper (giving the previously unpublished results of the author's own research based on management methods).
2. Survey paper (giving an original, detailed and critical view of a research problem or an area to which the author has made a contribution visible through his self-citation);
3. Short or preliminary communication (original management paper of full format but of a smaller extent or of a preliminary character);
4. Scientific critique or forum (discussion on a particular scientific topic, based exclusively on management argumentation) and commentaries. Exceptionally, in particular areas, a scientific paper in the Journal can be in a form of a monograph or a critical edition of scientific data (historical, archival, lexicographic, bibliographic, data survey, etc.) which were unknown or hardly accessible for scientific research.

**Professional articles:**

1. Professional paper (contribution offering experience useful for improvement of professional practice but not necessarily based on scientific methods);
2. Informative contribution (editorial, commentary, etc.);
3. Review (of a book, software, case study, scientific event, etc.)

**Language**

The article should be in English. The grammar and style of the article should be of good quality. The systematized text should be without abbreviations (except standard ones). All measurements must be in SI units. The sequence of formulae is denoted in Arabic numerals in parentheses on the right-hand side.

**Abstract and Summary**

An abstract is a concise informative presentation of the article content for fast and accurate Evaluation of its relevance. It is both in the Editorial Office's and the author's best interest for an abstract to contain terms often used for indexing and article search. The abstract describes the purpose of the study and the methods, outlines the findings and state the conclusions. A 100- to 250-Word abstract should be placed between the title and the keywords with the body text to follow. Besides an abstract are advised to have a summary in English, at the end of the article, after the Reference list. The summary should be structured and long up to 1/10 of the article length (it is more extensive than the abstract).

**Keywords**

Keywords are terms or phrases showing adequately the article content for indexing and search purposes. They should be allocated heaving in mind widely accepted international sources (index, dictionary or thesaurus), such as the Web of Science keyword list for science in general. The higher their usage frequency is the better. Up to 10 keywords immediately follow the abstract and the summary, in respective languages.

**Acknowledgements**

The name and the number of the project or programmed within which the article was realized is given in a separate note at the bottom of the first page together with the name of the institution which financially supported the project or programmed.

**Tables and Illustrations**

All the captions should be in the original language as well as in English, together with the texts in illustrations if possible. Tables are typed in the same style as the text and are denoted by numerals at the top. Photographs and drawings, placed appropriately in the text, should be clear, precise and suitable for reproduction. Drawings should be created in Word or Corel.

**Citation in the Text**

Citation in the text must be uniform. When citing references in the text, use the reference number set in square brackets from the Reference list at the end of the article.

**Footnotes**

Footnotes are given at the bottom of the page with the text they refer to. They can contain less relevant details, additional explanations or used sources (e.g. scientific material, manuals). They cannot replace the cited literature.

The article should be accompanied with a cover letter with the information about the author(s): surname, middle initial, first name, and citizen personal number, rank, title, e-mail address, and affiliation address, home address including municipality, phone number in the office and at home (or a mobile phone number). The cover letter should state the type of the article and tell which illustrations are original and which are not.

**Address of the Editorial Office:**

**Enriched Publications Pvt. Ltd.**  
S-9, IInd FLOOR, MLU POCKET,  
MANISH ABHINAV PLAZA-II, ABOVE FEDERAL BANK,  
PLOT NO-5, SECTOR -5, DWARKA, NEW DELHI, INDIA-110075,  
PHONE: - + (91)-(11)-45525005